

Dissociation cross sections of $\psi(3770)$, $\psi(4040)$, $\psi(4160)$, and $\psi(4415)$ mesons with nucleons

Ruo-Qing Ding¹, Xiao-Ming Xu¹, and H. J. Weber²

¹Department of Physics, Shanghai University, Baoshan, Shanghai 200444, China

²Department of Physics, University of Virginia, Charlottesville, VA 22904, USA

Abstract

We study the dissociation of $\psi(3770)$, $\psi(4040)$, $\psi(4160)$, and $\psi(4415)$ mesons in collisions with nucleons, which takes place in high-energy proton-nucleus collisions. Quark interchange between a nucleon and a $c\bar{c}$ meson leads to the dissociation of the $c\bar{c}$ meson. We consider the reactions: $pR \rightarrow \Lambda_c^+ \bar{D}^0$, $pR \rightarrow \Lambda_c^+ \bar{D}^{*0}$, $pR \rightarrow \Sigma_c^{++} D^-$, $pR \rightarrow \Sigma_c^{++} D^{*-}$, $pR \rightarrow \Sigma_c^+ \bar{D}^0$, $pR \rightarrow \Sigma_c^+ \bar{D}^{*0}$, $pR \rightarrow \Sigma_c^{*++} D^-$, $pR \rightarrow \Sigma_c^{*++} D^{*-}$, $pR \rightarrow \Sigma_c^{*+} \bar{D}^0$, and $pR \rightarrow \Sigma_c^{*+} \bar{D}^{*0}$, where R stands for $\psi(3770)$, $\psi(4040)$, $\psi(4160)$, or $\psi(4415)$. A reaction of a neutron and a $c\bar{c}$ meson corresponds to a reaction of a proton and the $c\bar{c}$ meson by replacing the up quark with the down quark and vice versa. Transition-amplitude formulas are derived from the S -matrix element. Unpolarized cross sections are calculated with the transition amplitudes for scattering in the prior form and in the post form. The cross sections relate to nodes in the radial wave functions of $\psi(3770)$, $\psi(4040)$, $\psi(4160)$, and $\psi(4415)$ mesons.

Keywords: Inelastic nucleon-charmonium scattering, quark interchange, relativistic constituent quark potential model.

PACS: 13.75.Lb; 12.39.Jh; 12.39.Pn

I. INTRODUCTION

It is shown in Refs. [1–3] that $\psi(3770)$, $\psi(4040)$, $\psi(4160)$, and $\psi(4415)$ mesons are the 1^3D_1 , 3^3S_1 , 2^3D_1 , and 4^3S_1 states of a charm quark and a charm antiquark. The four $c\bar{c}$ mesons have been widely studied in e^+e^- annihilation that produce hadrons [4–7], $\pi\pi J/\psi$ [8–10], $\eta J/\psi$ [9–12], $K^+K^- J/\psi$ [10], $\gamma\chi_{cJ}$ ($J = 1, 2$) [10, 13], two charmed mesons [14, 15], $D^0D^{*-}\pi^+$ [16], two charmed strange mesons [17, 18], $\pi\pi h_c$ [19], $\omega\chi_{c2}$ [20], $\mu^+\mu^-$ [21], and $\Lambda\bar{\Lambda}$ [22]. Electron-positron annihilation produces a virtual photon which splits into a charm quark and a charm antiquark, and this quark-antiquark pair becomes a $c\bar{c}$ meson nonperturbatively. Production of the $\psi(3770)$ meson in e^+e^- annihilation was studied in the nonrelativistic quantum chromodynamics (NRQCD) factorization formalism that includes color-singlet and color-octet contributions [23]. In Refs. [24, 25] the conversion of the photon to the $\psi(4040)$ or $\psi(4160)$ meson is indicated by a constant factor.

Au-Au collisions at the Relativistic Heavy Ion Collider (RHIC) and Pb-Pb collisions at the Large Hadron Collider (LHC) produce quark-gluon plasmas. At the critical temperature T_c the quark-gluon plasma becomes hadronic matter. Since $\psi(4040)$, $\psi(4160)$, and $\psi(4415)$ mesons are dissolved in hadronic matter when the temperature is larger than $0.97T_c$, $0.95T_c$, and $0.87T_c$, respectively [26], they can only be produced in hadronic matter. Therefore, the production of $\psi(4040)$, $\psi(4160)$, and $\psi(4415)$ can be taken as probes of hadronic matter that results from the quark-gluon plasma created in ultra-relativistic heavy-ion collisions. In hadronic matter they are produced in the following reactions: $D\bar{D} \rightarrow \rho R$, $D\bar{D}^* \rightarrow \pi R$, $D\bar{D}^* \rightarrow \rho R$, $D^*\bar{D}^* \rightarrow \pi R$, $D^*\bar{D}^* \rightarrow \rho R$ and so on, where R stands for $\psi(4040)$, $\psi(4160)$, or $\psi(4415)$. Charmed mesons have been well measured in Pb-Pb collisions at the LHC. It is shown in Ref. [27] that numbers of $\psi(4040)$, $\psi(4160)$, and $\psi(4415)$ produced in a central Pb-Pb collision at the center-of-mass energy per nucleon-nucleon pair $\sqrt{s_{NN}} = 5.02$ TeV are 0.25, 0.1, and 0.18, respectively. Therefore, it is interesting to measure $\psi(4040)$, $\psi(4160)$, and $\psi(4415)$ mesons produced in Pb-Pb collisions at the LHC.

Production of D -wave charmonia in nucleon-nucleon collisions was studied in NRQCD in Ref. [28]. Production cross sections depend on parton distribution functions, short-distance processes, and nonperturbative matrix elements of four-fermion operators. In

proton-nucleus reactions a charmonium produced in a proton-nucleon collision further interacts with other nucleons. The nucleon-charmonium collisions may break the charmonium, and thus reduce the charmonium number. Therefore, in the present work we study the dissociation of $\psi(3770)$, $\psi(4040)$, $\psi(4160)$, and $\psi(4415)$ mesons in collisions with nucleons. Since many experiments on pA reactions have been carried out at the RHIC and the LHC, it is interesting to study the dissociation processes.

$\psi(3770)$, $\psi(4040)$, $\psi(4160)$, and $\psi(4415)$ mesons are of special interest because they are easily produced at electron-positron colliders. The mechanism of producing them in proton-nucleus reactions is different from the mechanism of producing them in electron-positron collisions. The mesons are influenced by cold nuclear matter due to the dissociation processes and nuclear modification of parton distribution functions. Therefore, it will be interesting to compare the production of the mesons in proton-nucleus reactions with the production in electron-positron collisions in both experiment and theory in future.

This paper is organized as follows. In Sect. II we derive formulas of transition amplitudes which are used to calculate unpolarized cross sections for dissociation of $c\bar{c}$ mesons in collisions with nucleons. In Sect. III we present numerical cross sections along with relevant discussions. In Sect. IV we summarize the present work.

II. FORMALISM

We consider the reaction $A+B \rightarrow C+D$ where A and C represent baryons and B and D are mesons. Denote by E_i and \vec{P}_i (E_f and \vec{P}_f) the total energy and the total momentum of the initial (final) baryon and the initial (final) meson, respectively. If E_A (E_B , E_C , E_D) stands for the energy of hadron A (B , C , D), $E_i = E_A + E_B$ and $E_f = E_C + E_D$. Let H_I be the interaction potential between two constituents of hadrons in the reaction $A(q_1q_2q_3) + B(c\bar{c}) \rightarrow C(q_1q_2c) + D(q_3\bar{c})$, where q_1 , q_2 , and q_3 represent light quarks. Since the quark flavors inside baryon A differ from the charm flavor inside meson B , quark interchange (for example, q_3 and c) between baryon A and meson B gives rise to the

reaction. The S -matrix element for $A + B \rightarrow C + D$ is

$$S_{fi} = \delta_{fi} - 2\pi i \delta(E_f - E_i) \langle C, D | H_I | A, B \rangle. \quad (1)$$

Let $\vec{P}_{q_1 q_2 q_3}$ ($\vec{P}'_{q_1 q_2 c}$) and $\vec{R}_{q_1 q_2 q_3}$ ($\vec{R}_{q_1 q_2 c}$) be the total momentum and the center-of-mass coordinate of q_1 , q_2 , and q_3 (q_1 , q_2 , and c) in baryon A (C), respectively. Let $\vec{P}_{c\bar{c}}$ ($\vec{P}'_{q_3\bar{c}}$), $\vec{R}_{c\bar{c}}$ ($\vec{R}_{q_3\bar{c}}$), and $\vec{r}_{c\bar{c}}$ ($\vec{r}_{q_3\bar{c}}$) be the total momentum, the center-of-mass coordinate, and the relative coordinate of c and \bar{c} (q_3 and \bar{c}) of meson B (D), respectively. In case that quarks q_1 and q_2 have the same mass, we define

$$\vec{\rho} = \frac{1}{\sqrt{2}}(\vec{r}_{q_1} - \vec{r}_{q_2}), \quad (2)$$

and

$$\vec{\lambda}_i = \frac{1}{\sqrt{6}}(\vec{r}_{q_1} + \vec{r}_{q_2} - 2\vec{r}_{q_3}), \quad (3)$$

for baryon A , and

$$\vec{\lambda}_f = \frac{1}{\sqrt{6}}(\vec{r}_{q_1} + \vec{r}_{q_2} - 2\vec{r}_c), \quad (4)$$

for baryon C , where \vec{r}_{q_1} , \vec{r}_{q_2} , \vec{r}_{q_3} , and \vec{r}_c are the position vectors of quarks q_1 , q_2 , q_3 , and c , respectively. The wave function $|A, B\rangle$ of baryon A and meson B is

$$\psi_{AB} = \frac{e^{i\vec{P}_{q_1 q_2 q_3} \cdot \vec{R}_{q_1 q_2 q_3}}}{\sqrt{V}} \psi_{q_1 q_2 q_3}(\vec{\rho}, \vec{\lambda}_i) \frac{e^{i\vec{P}_{c\bar{c}} \cdot \vec{R}_{c\bar{c}}}}{\sqrt{V}} \psi_{c\bar{c}}(\vec{r}_{c\bar{c}}), \quad (5)$$

and the wave function $|C, D\rangle$ of baryon C and meson D is

$$\psi_{CD} = \frac{e^{i\vec{P}'_{q_1 q_2 c} \cdot \vec{R}_{q_1 q_2 c}}}{\sqrt{V}} \psi_{q_1 q_2 c}(\vec{\rho}, \vec{\lambda}_f) \frac{e^{i\vec{P}'_{q_3\bar{c}} \cdot \vec{R}_{q_3\bar{c}}}}{\sqrt{V}} \psi_{q_3\bar{c}}(\vec{r}_{q_3\bar{c}}), \quad (6)$$

in which V is the volume where every hadron wave function is normalized. $\psi_{q_1 q_2 q_3}(\vec{\rho}, \vec{\lambda}_i)$ ($\psi_{q_1 q_2 c}(\vec{\rho}, \vec{\lambda}_f)$) is the product of the color wave function, the flavor wave function, the spin wave function, and the space wave function of the three quarks. $\psi_{c\bar{c}}(\vec{r}_{c\bar{c}})$ ($\psi_{q_3\bar{c}}(\vec{r}_{q_3\bar{c}})$) is the product of the color wave function, the flavor wave function, the spin wave function, and the quark-antiquark relative-motion wave function.

With the wave functions we have

$$\langle C, D | H_I | A, B \rangle$$

$$\begin{aligned}
&= \int d^3 R_{q_1 q_2 q_3} d^3 \rho d^3 \lambda_i d^3 R_{c\bar{c}} d^3 r_{c\bar{c}} \psi_{CD}^+ H_1 \psi_{AB} \\
&= \int d^3 \rho d^3 \lambda_i d^3 r_{c\bar{c}} d^3 r_{q_1 q_2 q_3, c\bar{c}} d^3 R_{\text{total}} \\
&\quad \frac{\psi_{q_1 q_2 c}^+(\vec{\rho}, \vec{\lambda}_f)}{\sqrt{V}} \frac{\psi_{q_3 \bar{c}}^+(\vec{r}_{q_3 \bar{c}})}{\sqrt{V}} \exp(-i\vec{P}_f \cdot \vec{R}_{\text{total}} - i\vec{p}'_{q_1 q_2 c, q_3 \bar{c}} \cdot \vec{r}_{q_1 q_2 c, q_3 \bar{c}}) \\
&\quad H_1 \frac{\psi_{q_1 q_2 q_3}(\vec{\rho}, \vec{\lambda}_i)}{\sqrt{V}} \frac{\psi_{c\bar{c}}(\vec{r}_{c\bar{c}})}{\sqrt{V}} \exp(i\vec{P}_i \cdot \vec{R}_{\text{total}} + i\vec{p}_{q_1 q_2 q_3, c\bar{c}} \cdot \vec{r}_{q_1 q_2 q_3, c\bar{c}}) \\
&= (2\pi)^3 \delta^3(\vec{P}_f - \vec{P}_i) \int d^3 \rho d^3 \lambda_i d^3 r_{c\bar{c}} d^3 r_{q_1 q_2 q_3, c\bar{c}} \frac{\psi_{q_1 q_2 c}^+(\vec{\rho}, \vec{\lambda}_f)}{\sqrt{V}} \frac{\psi_{q_3 \bar{c}}^+(\vec{r}_{q_3 \bar{c}})}{\sqrt{V}} H_1 \\
&\quad \frac{\psi_{q_1 q_2 q_3}(\vec{\rho}, \vec{\lambda}_i)}{\sqrt{V}} \frac{\psi_{c\bar{c}}(\vec{r}_{c\bar{c}})}{\sqrt{V}} \exp(-i\vec{p}'_{q_1 q_2 c, q_3 \bar{c}} \cdot \vec{r}_{q_1 q_2 c, q_3 \bar{c}} + i\vec{p}_{q_1 q_2 q_3, c\bar{c}} \cdot \vec{r}_{q_1 q_2 q_3, c\bar{c}}) \\
&= (2\pi)^3 \delta^3(\vec{P}_f - \vec{P}_i) \frac{\mathcal{M}_{\text{fi}}}{V^2 \sqrt{2E_A 2E_B 2E_C 2E_D}}, \tag{7}
\end{aligned}$$

where $\vec{r}_{q_1 q_2 q_3, c\bar{c}}$ ($\vec{r}_{q_1 q_2 c, q_3 \bar{c}}$) and $\vec{p}_{q_1 q_2 q_3, c\bar{c}}$ ($\vec{p}'_{q_1 q_2 c, q_3 \bar{c}}$) are the relative coordinate and the relative momentum of $q_1 q_2 q_3$ and $c\bar{c}$ ($q_1 q_2 c$ and $q_3 \bar{c}$), respectively; \vec{R}_{total} is the center-of-mass coordinate of the two initial hadrons, i.e., of the two final hadrons; ψ_{CD}^+ is the Hermitean conjugate of ψ_{CD} ; \mathcal{M}_{fi} is the transition amplitude given by

$$\begin{aligned}
\mathcal{M}_{\text{fi}} &= \sqrt{2E_A 2E_B 2E_C 2E_D} \int d^3 \rho d^3 \lambda_i d^3 r_{c\bar{c}} d^3 r_{q_1 q_2 q_3, c\bar{c}} \psi_{q_1 q_2 c}^+(\vec{\rho}, \vec{\lambda}_f) \psi_{q_3 \bar{c}}^+(\vec{r}_{q_3 \bar{c}}) H_1 \\
&\quad \psi_{q_1 q_2 q_3}(\vec{\rho}, \vec{\lambda}_i) \psi_{c\bar{c}}(\vec{r}_{c\bar{c}}) \exp(-i\vec{p}'_{q_1 q_2 c, q_3 \bar{c}} \cdot \vec{r}_{q_1 q_2 c, q_3 \bar{c}} + i\vec{p}_{q_1 q_2 q_3, c\bar{c}} \cdot \vec{r}_{q_1 q_2 q_3, c\bar{c}}). \tag{8}
\end{aligned}$$

The wave function of baryon A and meson B is

$$\psi_{AB} = \phi_{A\text{color}} \phi_{B\text{color}} \phi_{A\text{flavor}} \phi_{B\text{flavor}} \phi_{A\text{space}} \chi_{S_A S_{A_z}} \phi_{B J_B J_{B_z}}, \tag{9}$$

and the wave function of baryon C and meson D is

$$\psi_{CD} = \phi_{C\text{color}} \phi_{D\text{color}} \phi_{C\text{flavor}} \phi_{D\text{flavor}} \phi_{C\text{space}} \phi_{D\text{rel}} \chi_{S_C S_{C_z}} \chi_{S_D S_{D_z}}, \tag{10}$$

where S_A (S_C , S_D) is the spin of hadron A (C , D) with its magnetic projection quantum number S_{A_z} (S_{C_z} , S_{D_z}); $\phi_{A\text{color}}$ ($\phi_{C\text{color}}$, $\phi_{D\text{color}}$), $\phi_{A\text{flavor}}$ ($\phi_{C\text{flavor}}$, $\phi_{D\text{flavor}}$), and $\chi_{S_A S_{A_z}}$ ($\chi_{S_C S_{C_z}}$, $\chi_{S_D S_{D_z}}$) are the color wave function, the flavor wave function, and the spin wave function of hadron A (C , D), respectively; $\phi_{A\text{space}}$ ($\phi_{C\text{space}}$) is the space wave function of baryon A (C); $\phi_{D\text{rel}}$ is the quark-antiquark relative-motion wave function of meson D ; $\phi_{B\text{color}}$, $\phi_{B\text{flavor}}$, and $\phi_{B J_B J_{B_z}}$ are the color wave function, the flavor wave function, and the space-spin wave function of meson B with the total angular momentum

J_B and its z component J_{Bz} , respectively. Denote by L_B and S_B the orbital angular momentum and the spin of meson B , respectively, and by M_B and S_{Bz} the magnetic projection quantum numbers of L_B and S_B . In Eq. (9) $\phi_{BJ_B J_{Bz}} = R_{L_B}(r_{c\bar{c}}) \sum_{M_B=-L_B}^{L_B} \sum_{S_{Bz}=-S_B}^{S_B} (L_B M_B S_B S_{Bz} | J_B J_{Bz}) Y_{L_B M_B} \chi_{S_B S_{Bz}}$ where $R_{L_B}(r_{c\bar{c}})$ is the radial wave function of the relative motion of c and \bar{c} , $(L_B M_B S_B S_{Bz} | J_B J_{Bz})$ are the Clebsch-Gordan coefficients, $Y_{L_B M_B}$ are the spherical harmonics, and $\chi_{S_B S_{Bz}}$ are the spin wave functions.

The interaction that governs scattering in the prior form shown in Fig. 1 is

$$H_I = V_{q_1\bar{c}} + V_{q_2\bar{c}} + V_{q_3\bar{c}} + V_{q_1c} + V_{q_2c} + V_{q_3c}, \quad (11)$$

and the interaction that governs scattering in the post form shown in Fig. 2 is

$$H_I = V_{q_1\bar{c}} + V_{q_2\bar{c}} + V_{c\bar{c}} + V_{q_1q_3} + V_{q_2q_3} + V_{q_3c}, \quad (12)$$

where V_{ab} is the potential between constituents a and b . Let $\vec{r}_{\bar{c}}$ be the position vector of antiquark \bar{c} . We take the Fourier transform of the potentials and wave functions:

$$V_{q_1\bar{c}}(\vec{r}_{q_1} - \vec{r}_{\bar{c}}) = \int \frac{d^3Q}{(2\pi)^3} V_{q_1\bar{c}}(\vec{Q}) e^{i\vec{Q}\cdot(\vec{r}_{q_1} - \vec{r}_{\bar{c}})}, \quad (13)$$

$$V_{q_2\bar{c}}(\vec{r}_{q_2} - \vec{r}_{\bar{c}}) = \int \frac{d^3Q}{(2\pi)^3} V_{q_2\bar{c}}(\vec{Q}) e^{i\vec{Q}\cdot(\vec{r}_{q_2} - \vec{r}_{\bar{c}})}, \quad (14)$$

$$V_{q_3\bar{c}}(\vec{r}_{q_3} - \vec{r}_{\bar{c}}) = \int \frac{d^3Q}{(2\pi)^3} V_{q_3\bar{c}}(\vec{Q}) e^{i\vec{Q}\cdot(\vec{r}_{q_3} - \vec{r}_{\bar{c}})}, \quad (15)$$

$$V_{q_1c}(\vec{r}_{q_1} - \vec{r}_c) = \int \frac{d^3Q}{(2\pi)^3} V_{q_1c}(\vec{Q}) e^{i\vec{Q}\cdot(\vec{r}_{q_1} - \vec{r}_c)}, \quad (16)$$

$$V_{q_2c}(\vec{r}_{q_2} - \vec{r}_c) = \int \frac{d^3Q}{(2\pi)^3} V_{q_2c}(\vec{Q}) e^{i\vec{Q}\cdot(\vec{r}_{q_2} - \vec{r}_c)}, \quad (17)$$

$$V_{q_3c}(\vec{r}_{q_3} - \vec{r}_c) = \int \frac{d^3Q}{(2\pi)^3} V_{q_3c}(\vec{Q}) e^{i\vec{Q}\cdot(\vec{r}_{q_3} - \vec{r}_c)}, \quad (18)$$

$$V_{c\bar{c}}(\vec{r}_c - \vec{r}_{\bar{c}}) = \int \frac{d^3Q}{(2\pi)^3} V_{c\bar{c}}(\vec{Q}) e^{i\vec{Q}\cdot(\vec{r}_c - \vec{r}_{\bar{c}})}, \quad (19)$$

$$V_{q_1q_3}(\vec{r}_{q_1} - \vec{r}_{q_3}) = \int \frac{d^3Q}{(2\pi)^3} V_{q_1q_3}(\vec{Q}) e^{i\vec{Q}\cdot(\vec{r}_{q_1} - \vec{r}_{q_3})}, \quad (20)$$

$$V_{q_2q_3}(\vec{r}_{q_2} - \vec{r}_{q_3}) = \int \frac{d^3Q}{(2\pi)^3} V_{q_2q_3}(\vec{Q}) e^{i\vec{Q}\cdot(\vec{r}_{q_2} - \vec{r}_{q_3})}, \quad (21)$$

$$\phi_{\text{Aspace}}(\vec{\rho}, \vec{\lambda}_i) = \int \frac{d^3 p_\rho}{(2\pi)^3} \frac{d^3 p_\lambda}{(2\pi)^3} \phi_{\text{Aspace}}(\vec{p}_\rho, \vec{p}_\lambda) e^{i\vec{p}_\rho \cdot \vec{\rho} + i\vec{p}_\lambda \cdot \vec{\lambda}_i}, \quad (22)$$

$$\phi_{B J_B J_{Bz}}(\vec{r}_{c\bar{c}}) = \int \frac{d^3 p_{c\bar{c}}}{(2\pi)^3} \phi_{B J_B J_{Bz}}(\vec{p}_{c\bar{c}}) e^{i\vec{p}_{c\bar{c}} \cdot \vec{r}_{c\bar{c}}}, \quad (23)$$

$$\phi_{\text{Cspace}}(\vec{\rho}, \vec{\lambda}_f) = \int \frac{d^3 p'_\rho}{(2\pi)^3} \frac{d^3 p'_\lambda}{(2\pi)^3} \phi_{\text{Cspace}}(\vec{p}'_\rho, \vec{p}'_\lambda) e^{i\vec{p}'_\rho \cdot \vec{\rho} + i\vec{p}'_\lambda \cdot \vec{\lambda}_f}, \quad (24)$$

$$\phi_{\text{Drel}}(\vec{r}_{q_3\bar{c}}) = \int \frac{d^3 p'_{q_3\bar{c}}}{(2\pi)^3} \phi_{\text{Drel}}(\vec{p}'_{q_3\bar{c}}) e^{i\vec{p}'_{q_3\bar{c}} \cdot \vec{r}_{q_3\bar{c}}}, \quad (25)$$

where \vec{Q} is the momentum attached to the dot-dashed lines in Figs. 1 and 2, $\vec{p}_{c\bar{c}}$ is the relative momentum of c and \bar{c} in meson B , and $\vec{p}'_{q_3\bar{c}}$ is the relative momentum of q_3 and \bar{c} in meson D . In momentum space the normalizations are

$$\int \frac{d^3 p_\rho}{(2\pi)^3} \int \frac{d^3 p_\lambda}{(2\pi)^3} \phi_{\text{Aspace}}^+(\vec{p}_\rho, \vec{p}_\lambda) \phi_{\text{Aspace}}(\vec{p}_\rho, \vec{p}_\lambda) = 1, \quad (26)$$

$$\int \frac{d^3 p_{c\bar{c}}}{(2\pi)^3} \phi_{B J_B J_{Bz}}^+(\vec{p}_{c\bar{c}}) \phi_{B J_B J_{Bz}}(\vec{p}_{c\bar{c}}) = 1, \quad (27)$$

$$\int \frac{d^3 p'_\rho}{(2\pi)^3} \int \frac{d^3 p'_\lambda}{(2\pi)^3} \phi_{\text{Cspace}}^+(\vec{p}'_\rho, \vec{p}'_\lambda) \phi_{\text{Cspace}}(\vec{p}'_\rho, \vec{p}'_\lambda) = 1, \quad (28)$$

$$\int \frac{d^3 p'_{q_3\bar{c}}}{(2\pi)^3} \phi_{\text{Drel}}^+(\vec{p}'_{q_3\bar{c}}) \phi_{\text{Drel}}(\vec{p}'_{q_3\bar{c}}) = 1. \quad (29)$$

When quarks q_1 and q_2 have equal masses, their masses are indicated by m . Let m_{q_3} , m_c , and $m_{\bar{c}}$ stand for the q_3 , c , and \bar{c} masses, respectively. From Eqs. (8)-(29) we obtain the transition amplitude for scattering in the prior form,

$$\begin{aligned} \mathcal{M}_{\text{fi}}^{\text{prior}} &= \sqrt{2E_A 2E_B 2E_C 2E_D} \phi_{\text{Ccolor}}^+ \phi_{\text{Dcolor}}^+ \phi_{\text{Cflavor}}^+ \phi_{\text{Dflavor}}^+ \chi_{S_C S_{Cz}}^+ \chi_{S_D S_{Dz}}^+ \\ &\int \frac{d^3 p'_\rho}{(2\pi)^3} \frac{d^3 p'_\lambda}{(2\pi)^3} \frac{d^3 p'_{q_3\bar{c}}}{(2\pi)^3} \phi_{\text{Cspace}}^+(\vec{p}'_\rho, \vec{p}'_\lambda) \phi_{\text{Drel}}^+(\vec{p}'_{q_3\bar{c}}) \\ &\left\{ V_{q_1\bar{c}} \left(\frac{2}{\sqrt{6}} \vec{p}'_\lambda + \vec{p}'_{q_3\bar{c}} - \vec{p}_{q_1 q_2 q_3, c\bar{c}} + o_{\text{r}} \vec{p}'_{q_1 q_2 c, q_3\bar{c}} \right) \right. \\ &\phi_{\text{Aspace}} \left(\vec{p}'_\rho - \frac{1}{\sqrt{3}} \vec{p}'_\lambda - \frac{\sqrt{2}}{2} \vec{p}'_{q_3\bar{c}} + \frac{\sqrt{2}}{2} \vec{p}_{q_1 q_2 q_3, c\bar{c}} - \frac{\sqrt{2} o_{\text{r}}}{2} \vec{p}'_{q_1 q_2 c, q_3\bar{c}}, \right. \\ &\left. \left. - \frac{\sqrt{6}}{2} \vec{p}'_{q_3\bar{c}} + \frac{\sqrt{6} m_{q_3}}{2(2m + m_{q_3})} \vec{p}_{q_1 q_2 q_3, c\bar{c}} + \frac{\sqrt{6} m_{q_3}}{2(m_{q_3} + m_{\bar{c}})} \vec{p}'_{q_1 q_2 c, q_3\bar{c}} \right) \right. \\ &\phi_{B J_B J_{Bz}} \left(-\frac{2}{\sqrt{6}} \vec{p}'_\lambda + \frac{m_c}{m_c + m_{\bar{c}}} \vec{p}_{q_1 q_2 q_3, c\bar{c}} + \frac{m_c}{2m + m_{\bar{c}}} \vec{p}'_{q_1 q_2 c, q_3\bar{c}} \right) \\ &\left. + V_{q_2\bar{c}} \left(\frac{2}{\sqrt{6}} \vec{p}'_\lambda + \vec{p}'_{q_3\bar{c}} - \vec{p}_{q_1 q_2 q_3, c\bar{c}} + o_{\text{r}} \vec{p}'_{q_1 q_2 c, q_3\bar{c}} \right) \right\} \end{aligned}$$

$$\begin{aligned}
& \phi_{\text{Aspace}} \left(\vec{p}'_\rho + \frac{1}{\sqrt{3}}\vec{p}'_\lambda + \frac{\sqrt{2}}{2}\vec{p}'_{q_3\bar{c}} - \frac{\sqrt{2}}{2}\vec{p}'_{q_1q_2q_3,c\bar{c}} + \frac{\sqrt{2}o_r}{2}\vec{p}'_{q_1q_2c,q_3\bar{c}}, \right. \\
& \quad \left. - \frac{\sqrt{6}}{2}\vec{p}'_{q_3\bar{c}} + \frac{\sqrt{6}m_{q_3}}{2(2m+m_{q_3})}\vec{p}'_{q_1q_2q_3,c\bar{c}} + \frac{\sqrt{6}m_{q_3}}{2(m_{q_3}+m_{\bar{c}})}\vec{p}'_{q_1q_2c,q_3\bar{c}} \right) \\
& \phi_{BJ_B J_{Bz}} \left(-\frac{2}{\sqrt{6}}\vec{p}'_\lambda + \frac{m_c}{m_c+m_{\bar{c}}}\vec{p}'_{q_1q_2q_3,c\bar{c}} + \frac{m_c}{2m+m_c}\vec{p}'_{q_1q_2c,q_3\bar{c}} \right) \\
& + V_{q_3\bar{c}} \left(\frac{2}{\sqrt{6}}\vec{p}'_\lambda + \vec{p}'_{q_3\bar{c}} - \vec{p}'_{q_1q_2q_3,c\bar{c}} + o_r\vec{p}'_{q_1q_2c,q_3\bar{c}} \right) \\
& \phi_{\text{Aspace}} \left(\vec{p}'_\rho, \vec{p}'_\lambda - \frac{\sqrt{6}m}{2m+m_{q_3}}\vec{p}'_{q_1q_2q_3,c\bar{c}} + \frac{\sqrt{6}m}{2m+m_c}\vec{p}'_{q_1q_2c,q_3\bar{c}} \right) \\
& \phi_{BJ_B J_{Bz}} \left(-\frac{2}{\sqrt{6}}\vec{p}'_\lambda + \frac{m_c}{m_c+m_{\bar{c}}}\vec{p}'_{q_1q_2q_3,c\bar{c}} + \frac{m_c}{2m+m_c}\vec{p}'_{q_1q_2c,q_3\bar{c}} \right) \\
& + V_{q_1c} \left(\frac{2}{\sqrt{6}}\vec{p}'_\lambda + \vec{p}'_{q_3\bar{c}} - \vec{p}'_{q_1q_2q_3,c\bar{c}} + o_r\vec{p}'_{q_1q_2c,q_3\bar{c}} \right) \\
& \phi_{\text{Aspace}} \left(\vec{p}'_\rho - \frac{1}{\sqrt{3}}\vec{p}'_\lambda - \frac{\sqrt{2}}{2}\vec{p}'_{q_3\bar{c}} + \frac{\sqrt{2}}{2}\vec{p}'_{q_1q_2q_3,c\bar{c}} - \frac{\sqrt{2}o_r}{2}\vec{p}'_{q_1q_2c,q_3\bar{c}}, \right. \\
& \quad \left. - \frac{\sqrt{6}}{2}\vec{p}'_{q_3\bar{c}} + \frac{\sqrt{6}m_{q_3}}{2(2m+m_{q_3})}\vec{p}'_{q_1q_2q_3,c\bar{c}} + \frac{\sqrt{6}m_{q_3}}{2(m_{q_3}+m_{\bar{c}})}\vec{p}'_{q_1q_2c,q_3\bar{c}} \right) \\
& \phi_{BJ_B J_{Bz}} \left(\vec{p}'_{q_3\bar{c}} - \frac{m_{\bar{c}}}{m_c+m_{\bar{c}}}\vec{p}'_{q_1q_2q_3,c\bar{c}} + \frac{m_{\bar{c}}}{m_{q_3}+m_{\bar{c}}}\vec{p}'_{q_1q_2c,q_3\bar{c}} \right) \\
& + V_{q_2c} \left(\frac{2}{\sqrt{6}}\vec{p}'_\lambda + \vec{p}'_{q_3\bar{c}} - \vec{p}'_{q_1q_2q_3,c\bar{c}} + o_r\vec{p}'_{q_1q_2c,q_3\bar{c}} \right) \\
& \phi_{\text{Aspace}} \left(\vec{p}'_\rho + \frac{1}{\sqrt{3}}\vec{p}'_\lambda + \frac{\sqrt{2}}{2}\vec{p}'_{q_3\bar{c}} - \frac{\sqrt{2}}{2}\vec{p}'_{q_1q_2q_3,c\bar{c}} + \frac{\sqrt{2}o_r}{2}\vec{p}'_{q_1q_2c,q_3\bar{c}}, \right. \\
& \quad \left. - \frac{\sqrt{6}}{2}\vec{p}'_{q_3\bar{c}} + \frac{\sqrt{6}m_{q_3}}{2(2m+m_{q_3})}\vec{p}'_{q_1q_2q_3,c\bar{c}} + \frac{\sqrt{6}m_{q_3}}{2(m_{q_3}+m_{\bar{c}})}\vec{p}'_{q_1q_2c,q_3\bar{c}} \right) \\
& \phi_{BJ_B J_{Bz}} \left(\vec{p}'_{q_3\bar{c}} - \frac{m_{\bar{c}}}{m_c+m_{\bar{c}}}\vec{p}'_{q_1q_2q_3,c\bar{c}} + \frac{m_{\bar{c}}}{m_{q_3}+m_{\bar{c}}}\vec{p}'_{q_1q_2c,q_3\bar{c}} \right) \\
& + V_{q_3c} \left(\frac{2}{\sqrt{6}}\vec{p}'_\lambda + \vec{p}'_{q_3\bar{c}} - \vec{p}'_{q_1q_2q_3,c\bar{c}} + o_r\vec{p}'_{q_1q_2c,q_3\bar{c}} \right) \\
& \phi_{\text{Aspace}} \left(\vec{p}'_\rho, \vec{p}'_\lambda - \frac{\sqrt{6}m}{2m+m_{q_3}}\vec{p}'_{q_1q_2q_3,c\bar{c}} + \frac{\sqrt{6}m}{2m+m_c}\vec{p}'_{q_1q_2c,q_3\bar{c}} \right) \\
& \left. \phi_{BJ_B J_{Bz}} \left(\vec{p}'_{q_3\bar{c}} - \frac{m_{\bar{c}}}{m_c+m_{\bar{c}}}\vec{p}'_{q_1q_2q_3,c\bar{c}} + \frac{m_{\bar{c}}}{m_{q_3}+m_{\bar{c}}}\vec{p}'_{q_1q_2c,q_3\bar{c}} \right) \right\} \\
& \phi_{\text{Acolor}}\phi_{\text{Bcolor}}\phi_{\text{Aflavor}}\phi_{\text{Bflavor}}\chi_{S_A S_{A_z}}, \tag{30}
\end{aligned}$$

with $o_r = (2mm_{\bar{c}} - m_{q_3}m_c)/[(2m+m_c)(m_{q_3}+m_{\bar{c}})]$, and the transition amplitude for

scattering in the post form,

$$\begin{aligned}
\mathcal{M}_{\text{fi}}^{\text{post}} &= \sqrt{2E_A 2E_B 2E_C 2E_D} \phi_{C\text{color}}^+ \phi_{D\text{color}}^+ \phi_{C\text{flavor}}^+ \phi_{D\text{flavor}}^+ \chi_{S_C S_C z}^+ \chi_{S_D S_D z}^+ \\
&\int \frac{d^3 p'_\rho}{(2\pi)^3} \frac{d^3 p'_\lambda}{(2\pi)^3} \frac{d^3 p'_{q_3 \bar{c}}}{(2\pi)^3} \phi_{C\text{space}}^+(\vec{p}'_\rho, \vec{p}'_\lambda) \phi_{D\text{rel}}^+(\vec{p}'_{q_3 \bar{c}}) \\
&\left\{ V_{q_1 \bar{c}} \left(\frac{2}{\sqrt{6}} \vec{p}'_\lambda + \vec{p}'_{q_3 \bar{c}} - \vec{p}_{q_1 q_2 q_3, c \bar{c}} + o_r \vec{p}'_{q_1 q_2 c, q_3 \bar{c}} \right) \right. \\
&\phi_{A\text{space}} \left(\vec{p}'_\rho - \frac{1}{\sqrt{3}} \vec{p}'_\lambda - \frac{\sqrt{2}}{2} \vec{p}'_{q_3 \bar{c}} + \frac{\sqrt{2}}{2} \vec{p}_{q_1 q_2 q_3, c \bar{c}} - \frac{\sqrt{2} o_r}{2} \vec{p}'_{q_1 q_2 c, q_3 \bar{c}}, \right. \\
&\left. - \frac{\sqrt{6}}{2} \vec{p}'_{q_3 \bar{c}} + \frac{\sqrt{6} m_{q_3}}{2(2m + m_{q_3})} \vec{p}_{q_1 q_2 q_3, c \bar{c}} + \frac{\sqrt{6} m_{q_3}}{2(m_{q_3} + m_{\bar{c}})} \vec{p}'_{q_1 q_2 c, q_3 \bar{c}} \right) \\
&\phi_{B J_B J_{Bz}} \left(-\frac{2}{\sqrt{6}} \vec{p}'_\lambda + \frac{m_c}{m_c + m_{\bar{c}}} \vec{p}_{q_1 q_2 q_3, c \bar{c}} + \frac{m_c}{2m + m_c} \vec{p}'_{q_1 q_2 c, q_3 \bar{c}} \right) \\
&+ V_{q_2 \bar{c}} \left(\frac{2}{\sqrt{6}} \vec{p}'_\lambda + \vec{p}'_{q_3 \bar{c}} - \vec{p}_{q_1 q_2 q_3, c \bar{c}} + o_r \vec{p}'_{q_1 q_2 c, q_3 \bar{c}} \right) \\
&\phi_{A\text{space}} \left(\vec{p}'_\rho + \frac{1}{\sqrt{3}} \vec{p}'_\lambda + \frac{\sqrt{2}}{2} \vec{p}'_{q_3 \bar{c}} - \frac{\sqrt{2}}{2} \vec{p}_{q_1 q_2 q_3, c \bar{c}} + \frac{\sqrt{2} o_r}{2} \vec{p}'_{q_1 q_2 c, q_3 \bar{c}}, \right. \\
&\left. - \frac{\sqrt{6}}{2} \vec{p}'_{q_3 \bar{c}} + \frac{\sqrt{6} m_{q_3}}{2(2m + m_{q_3})} \vec{p}_{q_1 q_2 q_3, c \bar{c}} + \frac{\sqrt{6} m_{q_3}}{2(m_{q_3} + m_{\bar{c}})} \vec{p}'_{q_1 q_2 c, q_3 \bar{c}} \right) \\
&\phi_{B J_B J_{Bz}} \left(-\frac{2}{\sqrt{6}} \vec{p}'_\lambda + \frac{m_c}{m_c + m_{\bar{c}}} \vec{p}_{q_1 q_2 q_3, c \bar{c}} + \frac{m_c}{2m + m_c} \vec{p}'_{q_1 q_2 c, q_3 \bar{c}} \right) \\
&+ V_{q_3 c} \left(\frac{2}{\sqrt{6}} \vec{p}'_\lambda + \vec{p}'_{q_3 \bar{c}} - \vec{p}_{q_1 q_2 q_3, c \bar{c}} + o_r \vec{p}'_{q_1 q_2 c, q_3 \bar{c}} \right) \\
&\phi_{A\text{space}} \left(\vec{p}'_\rho, \vec{p}'_\lambda - \frac{\sqrt{6} m}{2m + m_{q_3}} \vec{p}_{q_1 q_2 q_3, c \bar{c}} + \frac{\sqrt{6} m}{2m + m_c} \vec{p}'_{q_1 q_2 c, q_3 \bar{c}} \right) \\
&\left. \phi_{B J_B J_{Bz}} \left(\vec{p}'_{q_3 \bar{c}} - \frac{m_{\bar{c}}}{m_c + m_{\bar{c}}} \vec{p}_{q_1 q_2 q_3, c \bar{c}} + \frac{m_{\bar{c}}}{m_{q_3} + m_{\bar{c}}} \vec{p}'_{q_1 q_2 c, q_3 \bar{c}} \right) \right\} \\
&\phi_{A\text{color}} \phi_{B\text{color}} \phi_{A\text{flavor}} \phi_{B\text{flavor}} \chi_{S_A S_A z} \\
&+ \sqrt{2E_A 2E_B 2E_C 2E_D} \phi_{C\text{color}}^+ \phi_{D\text{color}}^+ \phi_{C\text{flavor}}^+ \phi_{D\text{flavor}}^+ \chi_{S_C S_C z}^+ \chi_{S_D S_D z}^+ \\
&\int \frac{d^3 p_\rho}{(2\pi)^3} \frac{d^3 p_\lambda}{(2\pi)^3} \frac{d^3 p_{c \bar{c}}}{(2\pi)^3} \\
&\left\{ \phi_{C\text{space}}^+ \left(\vec{p}_\rho, \vec{p}_\lambda + \frac{\sqrt{6} m}{2m + m_{q_3}} \vec{p}_{q_1 q_2 q_3, c \bar{c}} - \frac{\sqrt{6} m}{2m + m_c} \vec{p}'_{q_1 q_2 c, q_3 \bar{c}} \right) \right. \\
&\phi_{D\text{rel}}^+ \left(-\frac{2}{\sqrt{6}} \vec{p}_\lambda + \frac{m_{q_3}}{2m + m_{q_3}} \vec{p}_{q_1 q_2 q_3, c \bar{c}} + \frac{m_{q_3}}{m_{q_3} + m_{\bar{c}}} \vec{p}'_{q_1 q_2 c, q_3 \bar{c}} \right) \\
&\left. V_{c \bar{c}} \left(-\frac{2}{\sqrt{6}} \vec{p}_\lambda - \vec{p}_{c \bar{c}} - o_t \vec{p}_{q_1 q_2 q_3, c \bar{c}} + \vec{p}'_{q_1 q_2 c, q_3 \bar{c}} \right) \right\}
\end{aligned}$$

$$\begin{aligned}
& +\phi_{C\text{space}}^+ \left(\vec{p}_\rho - \frac{1}{\sqrt{3}}\vec{p}_\lambda - \frac{\sqrt{2}}{2}\vec{p}_{c\bar{c}} - \frac{\sqrt{2}o_t}{2}\vec{p}_{q_1q_2q_3,c\bar{c}} + \frac{\sqrt{2}}{2}\vec{p}'_{q_1q_2c,q_3\bar{c}}, \right. \\
& \quad \left. -\frac{\sqrt{6}}{2}\vec{p}_{c\bar{c}} + \frac{\sqrt{6}m_c}{2(m_c+m_{\bar{c}})}\vec{p}_{q_1q_2q_3,c\bar{c}} + \frac{\sqrt{6}m_c}{2(2m+m_c)}\vec{p}'_{q_1q_2c,q_3\bar{c}} \right) \\
& \phi_{D\text{rel}}^+ \left(\vec{p}_{c\bar{c}} + \frac{m_{\bar{c}}}{m_c+m_{\bar{c}}}\vec{p}_{q_1q_2q_3,c\bar{c}} - \frac{m_{\bar{c}}}{m_{q_3}+m_{\bar{c}}}\vec{p}'_{q_1q_2c,q_3\bar{c}} \right) \\
& V_{q_1q_3} \left(-\frac{2}{\sqrt{6}}\vec{p}_\lambda - \vec{p}_{c\bar{c}} - o_t\vec{p}_{q_1q_2q_3,c\bar{c}} + \vec{p}'_{q_1q_2c,q_3\bar{c}} \right) \\
& +\phi_{C\text{space}}^+ \left(\vec{p}_\rho + \frac{1}{\sqrt{3}}\vec{p}_\lambda + \frac{\sqrt{2}}{2}\vec{p}_{c\bar{c}} + \frac{\sqrt{2}o_t}{2}\vec{p}_{q_1q_2q_3,c\bar{c}} - \frac{\sqrt{2}}{2}\vec{p}'_{q_1q_2c,q_3\bar{c}}, \right. \\
& \quad \left. -\frac{\sqrt{6}}{2}\vec{p}_{c\bar{c}} + \frac{\sqrt{6}m_c}{2(m_c+m_{\bar{c}})}\vec{p}_{q_1q_2q_3,c\bar{c}} + \frac{\sqrt{6}m_c}{2(2m+m_c)}\vec{p}'_{q_1q_2c,q_3\bar{c}} \right) \\
& \phi_{D\text{rel}}^+ \left(\vec{p}_{c\bar{c}} + \frac{m_{\bar{c}}}{m_c+m_{\bar{c}}}\vec{p}_{q_1q_2q_3,c\bar{c}} - \frac{m_{\bar{c}}}{m_{q_3}+m_{\bar{c}}}\vec{p}'_{q_1q_2c,q_3\bar{c}} \right) \\
& V_{q_2q_3} \left(-\frac{2}{\sqrt{6}}\vec{p}_\lambda - \vec{p}_{c\bar{c}} - o_t\vec{p}_{q_1q_2q_3,c\bar{c}} + \vec{p}'_{q_1q_2c,q_3\bar{c}} \right) \Big\} \\
& \phi_{A\text{space}}(\vec{p}_\rho, \vec{p}_\lambda)\phi_{BJ_BJ_{Bz}}(\vec{p}_{c\bar{c}})\phi_{A\text{color}}\phi_{B\text{color}}\phi_{A\text{flavor}}\phi_{B\text{flavor}}\chi_{S_A S_{A_z}}. \tag{31}
\end{aligned}$$

with $o_t = (2mm_{\bar{c}} - m_{q_3}m_c)/[(m_c + m_{\bar{c}})(2m + m_{q_3})]$. The variables \vec{p}_ρ and \vec{p}_λ in $\phi_{A\text{space}}(\vec{p}_\rho, \vec{p}_\lambda)$, $\vec{p}_{c\bar{c}}$ in $\phi_{BJ_BJ_{Bz}}(\vec{p}_{c\bar{c}})$, \vec{p}'_ρ and \vec{p}'_λ in $\phi_{C\text{space}}(\vec{p}'_\rho, \vec{p}'_\lambda)$, and $\vec{p}'_{q_3\bar{c}}$ in $\phi_{D\text{rel}}(\vec{p}'_{q_3\bar{c}})$ equal the expressions enclosed by the parentheses that follow $\phi_{A\text{space}}$, $\phi_{BJ_BJ_{Bz}}$, $\phi_{C\text{space}}$, and $\phi_{D\text{rel}}$.

With the transition amplitudes the unpolarized cross section for $A + B \rightarrow C + D$ is

$$\begin{aligned}
\sigma^{\text{unpol}}(\sqrt{s}) &= \frac{1}{(2J_A + 1)(2J_B + 1)} \frac{1}{64\pi s} \frac{|\vec{P}'(\sqrt{s})|}{|\vec{P}(\sqrt{s})|} \\
& \int_0^\pi d\theta \sum_{J_{Az}J_{Bz}J_{Cz}J_{Dz}} (|\mathcal{M}_{\text{fi}}^{\text{prior}}|^2 + |\mathcal{M}_{\text{fi}}^{\text{post}}|^2) \sin\theta, \tag{32}
\end{aligned}$$

where s is the Mandelstam variable obtained from the four-momenta P_A and P_B of hadrons A and B by $s = (P_A + P_B)^2$; J_A (J_B , J_C , J_D) and J_{Az} (J_{Bz} , J_{Cz} , J_{Dz}) of hadron A (B , C , D) are the total angular momentum and its z component, respectively; θ is the angle between \vec{P} and \vec{P}' which are the three-dimensional momentum components of baryons A and C in the center-of-momentum frame of the initial baryon and the initial meson, respectively. We calculate the cross section in the center-of-momentum frame.

III. NUMERICAL CROSS SECTIONS AND DISCUSSIONS

We use the notation $D = \begin{pmatrix} D^+ \\ D^0 \end{pmatrix}$, $\bar{D} = \begin{pmatrix} \bar{D}^0 \\ D^- \end{pmatrix}$, $D^* = \begin{pmatrix} D^{*+} \\ D^{*0} \end{pmatrix}$, and $\bar{D}^* = \begin{pmatrix} \bar{D}^{*0} \\ D^{*-} \end{pmatrix}$. We consider the following reactions:

$$\begin{aligned}
pR &\rightarrow \Lambda_c^+ \bar{D}^0, & pR &\rightarrow \Lambda_c^+ \bar{D}^{*0}, \\
pR &\rightarrow \Sigma_c^{++} D^-, & pR &\rightarrow \Sigma_c^{++} D^{*-}, \\
pR &\rightarrow \Sigma_c^+ \bar{D}^0, & pR &\rightarrow \Sigma_c^+ \bar{D}^{*0}, \\
pR &\rightarrow \Sigma_c^{*++} D^-, & pR &\rightarrow \Sigma_c^{*++} D^{*-}, \\
pR &\rightarrow \Sigma_c^{*+} \bar{D}^0, & pR &\rightarrow \Sigma_c^{*+} \bar{D}^{*0},
\end{aligned}$$

where R stands for $\psi(3770)$, $\psi(4040)$, $\psi(4160)$, or $\psi(4415)$. By replacing the up quark with the down quark and vice versa in these ten reactions, they give ten reactions of a neutron and a $c\bar{c}$ meson. Since the cross section for $nR \rightarrow \Lambda_c^+ D^-$ ($nR \rightarrow \Lambda_c^+ D^{*-}$, $nR \rightarrow \Sigma_c^0 \bar{D}^0$, $nR \rightarrow \Sigma_c^0 \bar{D}^{*0}$, $nR \rightarrow \Sigma_c^+ D^-$, $nR \rightarrow \Sigma_c^+ D^{*-}$, $nR \rightarrow \Sigma_c^{*0} \bar{D}^0$, $nR \rightarrow \Sigma_c^{*0} \bar{D}^{*0}$, $nR \rightarrow \Sigma_c^{*+} D^-$, $nR \rightarrow \Sigma_c^{*+} D^{*-}$) equals the one for $pR \rightarrow \Lambda_c^+ \bar{D}^0$ ($pR \rightarrow \Lambda_c^+ \bar{D}^{*0}$, $pR \rightarrow \Sigma_c^{++} D^-$, $pR \rightarrow \Sigma_c^{++} D^{*-}$, $pR \rightarrow \Sigma_c^+ \bar{D}^0$, $pR \rightarrow \Sigma_c^+ \bar{D}^{*0}$, $pR \rightarrow \Sigma_c^{*++} D^-$, $pR \rightarrow \Sigma_c^{*++} D^{*-}$, $pR \rightarrow \Sigma_c^{*+} \bar{D}^0$, $pR \rightarrow \Sigma_c^{*+} \bar{D}^{*0}$), it is enough to only discuss reactions of the proton and the $c\bar{c}$ meson in this section. We calculate unpolarized cross sections for these reactions with Eq. (32). As seen in Eqs. (30) and (31), $\mathcal{M}_{\text{fi}}^{\text{prior}}$ and $\mathcal{M}_{\text{fi}}^{\text{post}}$ used in Eq. (32) involve $\phi_{BJ_B J_{Bz}}$ and $\phi_{D\text{rel}}$. The two wave functions are obtained from solutions of the Schrödinger equation with the potential between constituents a and b in coordinate space,

$$\begin{aligned}
V_{ab}(\vec{r}_{ab}) &= -\frac{\vec{\lambda}_a}{2} \cdot \frac{\vec{\lambda}_b}{2} \frac{3}{4} k r_{ab} + \frac{\vec{\lambda}_a}{2} \cdot \frac{\vec{\lambda}_b}{2} \frac{6\pi}{25} \frac{v(\lambda r_{ab})}{r_{ab}} \\
&- \frac{\vec{\lambda}_a}{2} \cdot \frac{\vec{\lambda}_b}{2} \frac{16\pi^2}{25} \frac{d^3}{\pi^{3/2}} \exp(-d^2 r_{ab}^2) \frac{\vec{s}_a \cdot \vec{s}_b}{m_a m_b} + \frac{\vec{\lambda}_a}{2} \cdot \frac{\vec{\lambda}_b}{2} \frac{4\pi}{25} \frac{1}{r_{ab}} \frac{d^2 v(\lambda r_{ab})}{dr_{ab}^2} \frac{\vec{s}_a \cdot \vec{s}_b}{m_a m_b} \\
&- \frac{\vec{\lambda}_a}{2} \cdot \frac{\vec{\lambda}_b}{2} \frac{6\pi}{25 m_a m_b} \left[v(\lambda r_{ab}) - r_{ab} \frac{dv(\lambda r_{ab})}{dr_{ab}} + \frac{r_{ab}^2}{3} \frac{d^2 v(\lambda r_{ab})}{dr_{ab}^2} \right] \\
&\left(\frac{3\vec{s}_a \cdot \vec{r}_{ab} \vec{s}_b \cdot \vec{r}_{ab}}{r_{ab}^5} - \frac{\vec{s}_a \cdot \vec{s}_b}{r_{ab}^3} \right), \tag{33}
\end{aligned}$$

where \vec{r}_{ab} is the relative coordinate of constituents a and b ; $k = 0.153 \text{ GeV}^2$ and $\lambda = 0.39 \text{ GeV}$; m_a , \vec{s}_a , and $\vec{\lambda}_a$ are individually the mass, the spin, and the Gell-Mann matrices for the color generators of constituent a ; the function v is given by Buchmüller and Tye in Ref. [29]; the quantity d is

$$d^2 = d_\alpha^2 \left[\frac{1}{2} + \frac{1}{2} \left(\frac{4m_a m_b}{(m_a + m_b)^2} \right)^4 \right] + d_\beta^2 \left(\frac{2m_a m_b}{m_a + m_b} \right)^2, \quad (34)$$

where $d_\alpha = 0.34 \text{ GeV}$ and $d_\beta = 0.45$. The potential originates from quantum chromodynamics (QCD) [29]. The first two terms are the Buchmüller-Tye potential, and the other terms come from one-gluon exchange plus perturbative one- and two-loop corrections [30].

The function $v(x)$ manifests one-gluon exchange plus perturbative one- and two-loop corrections between constituents a and b . It increases from 0 to 1 when x increases from 0 to the positive infinity. Consequently, the second term is not a color Coulomb potential.

One-gluon exchange between two constituents gives rise to the Fermi contact term $-\frac{\vec{\lambda}_a \cdot \vec{\lambda}_b}{2} \cdot \frac{\vec{s}_a \cdot \vec{s}_b}{2} \frac{16\pi^2}{25} \delta^3(\vec{r}_{ab}) \frac{\vec{s}_a \cdot \vec{s}_b}{m_a m_b}$. The $\delta^3(\vec{r}_{ab})$ function fixes the positions of the two constituents to $\vec{r}_{ab} = 0$. However, the constituent positions fluctuate in the presence of one- and two-loop corrections. To allow the position fluctuation, $\delta^3(\vec{r}_{ab})$ is replaced with $\frac{d^3}{\pi^{3/2}} \exp(-d^2 r_{ab}^2)$ so as to arrive at the third term on the right-hand side of Eq. (33), which is the smearing of the Fermi contact term [1]. The Gaussian has a width of $2\sqrt{\ln 2}/d$, and d^{-1} indicates the fluctuation size. The larger is d , the smaller is the fluctuation size. d depends on constituent masses. When $m_a = m_b$, $d^2 = d_\alpha^2 + d_\beta^2 m_b^2$. When $m_a \gg m_b$, $d^2 \approx d_\alpha^2/2 + 4d_\beta^2 m_b^2$. In the two cases the d_α term gives a constant value to d , and the d_β term is proportional to m_b^2 . The two terms provide different mass dependence. Since $d^2 > d_\alpha^2/2$, the parameter d_α reflects the fact that in a confined system the smearing must be limited.

The masses of the up quark, the down quark, the strange quark, and the charm quark are 0.32 GeV, 0.32 GeV, 0.5 GeV, and 1.51 GeV, respectively. Solving the Schrödinger equation with V_{ab} , we obtain meson masses that are close to the experimental masses of π , ρ , K , K^* , D , D^* , D_s , D_s^* , J/ψ , χ_c , ψ' , $\psi(3770)$, $\psi(4040)$, $\psi(4160)$, and $\psi(4415)$ mesons listed in Ref. [31]. The experimental data of S -wave $I = 2$ elastic phase shifts for $\pi\pi$ scattering [32] are reproduced in the Born approximation.

$\mathcal{M}_{\text{fi}}^{\text{prior}}$ and $\mathcal{M}_{\text{fi}}^{\text{post}}$ involve the space wave functions ϕ_{Aspace} and ϕ_{Cspace} . The space wave functions of ground-state baryons are usually assumed to be harmonic-oscillator wave functions [33, 34]:

$$\phi_{\text{Aspace}}(\vec{\rho}, \vec{\lambda}_i) = \left(\frac{\alpha_\rho \alpha_{\lambda_i}}{\pi}\right)^{1.5} \exp\left(-\frac{\alpha_\rho^2 \vec{\rho}^2 + \alpha_{\lambda_i}^2 \vec{\lambda}_i^2}{2}\right), \quad (35)$$

and $\phi_{\text{Cspace}}(\vec{\rho}, \vec{\lambda}_f)$ is obtained from $\phi_{\text{Aspace}}(\vec{\rho}, \vec{\lambda}_i)$ by replacing λ_i with λ_f . The wave function $\psi_{q_1 q_2 q_3}(\vec{\rho}, \vec{\lambda}_i)$ in Eq. (5) is

$$\psi_{q_1 q_2 q_3}(\vec{\rho}, \vec{\lambda}_i) = \phi_{\text{Acolor}} \phi_{\text{Aflavor}} \phi_{\text{Aspace}}(\vec{\rho}, \vec{\lambda}_i) \chi_{S_A S_{A_z}}, \quad (36)$$

and $\psi_{q_1 q_2 c}$ in Eq. (6) is given from $\psi_{q_1 q_2 q_3}$ by replacing q_3 ($\vec{\lambda}_i, A$) with c ($\vec{\lambda}_f, C$). Masses of baryons in the baryon octet and the baryon decuplet are given by

$$m_{\text{B}} = 2m + m_{q_3} + \int d^3 \rho d^3 \lambda_i \psi_{q_1 q_2 q_3}^+(\vec{\rho}, \vec{\lambda}_i) \left[\frac{\vec{\nabla}_{\vec{\rho}}^2}{2m} + \frac{\vec{\nabla}_{\vec{\lambda}_i}^2}{2m_{\lambda_i}} + V_{q_1 q_2}(\vec{r}_{q_1 q_2}) + V_{q_2 q_3}(\vec{r}_{q_2 q_3}) + V_{q_3 q_1}(\vec{r}_{q_3 q_1}) \right] \psi_{q_1 q_2 q_3}(\vec{\rho}, \vec{\lambda}_i), \quad (37)$$

with $m_{\lambda_i} = \frac{3mm_{q_3}}{2m+m_{q_3}}$. Replacing q_3 ($\vec{\lambda}_i$) with c ($\vec{\lambda}_f$), Eq. (37) is used to calculate masses of ground-state charmed baryons. Let $m_p, m_{\Lambda_c^+}, m_{\Sigma_c^{++}}, m_{\Sigma_c^+}, m_{\Sigma_c^{*++}},$ and $m_{\Sigma_c^{*+}}$ represent the experimental masses of $p, \Lambda_c^+, \Sigma_c^{++}, \Sigma_c^+, \Sigma_c^{*++},$ and Σ_c^{*+} baryons, respectively. Fits to the experimental masses of the six baryons give

$$\begin{aligned} \alpha_\rho &= 0.3 \text{ GeV}, & \alpha_{\lambda_i} &= 0.3 \text{ GeV}, & m_p &= 0.938272 \text{ GeV}; \\ \alpha_\rho &= 0.222594 \text{ GeV}, & \alpha_{\lambda_f} &= 0.43 \text{ GeV}, & m_{\Lambda_c^+} &= 2.28646 \text{ GeV}; \\ \alpha_\rho &= 0.196273 \text{ GeV}, & \alpha_{\lambda_f} &= 0.43 \text{ GeV}, & m_{\Sigma_c^{++}} &= 2.45397 \text{ GeV}; \\ \alpha_\rho &= 0.19642 \text{ GeV}, & \alpha_{\lambda_f} &= 0.43 \text{ GeV}, & m_{\Sigma_c^+} &= 2.4529 \text{ GeV}; \\ \alpha_\rho &= 0.19092 \text{ GeV}, & \alpha_{\lambda_f} &= 0.43 \text{ GeV}, & m_{\Sigma_c^{*++}} &= 2.51841 \text{ GeV}; \\ \alpha_\rho &= 0.19105 \text{ GeV}, & \alpha_{\lambda_f} &= 0.43 \text{ GeV}, & m_{\Sigma_c^{*+}} &= 2.5175 \text{ GeV}. \end{aligned}$$

Using the mesonic quark-antiquark relative-motion wave functions and the space wave functions of baryons, we obtain unpolarized cross sections for dissociation of $\psi(3770)$,

$\psi(4040)$, $\psi(4160)$, and $\psi(4415)$ mesons in collisions with protons. The cross sections are plotted in Figs. 3-12, and are parametrized as

$$\sigma^{\text{unpol}}(\sqrt{s}) = \frac{\vec{P}^{\prime 2}}{\vec{P}^2} \left\{ a_1 \left(\frac{\sqrt{s} - \sqrt{s_0}}{b_1} \right)^{c_1} \exp \left[c_1 \left(1 - \frac{\sqrt{s} - \sqrt{s_0}}{b_1} \right) \right] + a_2 \left(\frac{\sqrt{s} - \sqrt{s_0}}{b_2} \right)^{c_2} \exp \left[c_2 \left(1 - \frac{\sqrt{s} - \sqrt{s_0}}{b_2} \right) \right] \right\}, \quad (38)$$

where $\sqrt{s_0}$ is the threshold energy, and a_1 , b_1 , c_1 , a_2 , b_2 , and c_2 are parameters. The parameter values are listed in Tables 1-2. The threshold energy of inelastic $p + \psi(3770)$ ($p + \psi(4040)$, $p + \psi(4160)$, $p + \psi(4415)$) scattering is the sum of the proton and $\psi(3770)$ ($\psi(4040)$, $\psi(4160)$, $\psi(4415)$) masses. At the threshold energy $|\vec{P}|$ in Eq. (32) equals zero, but $|\vec{P}'|$ does not. The cross section is thus infinite at the threshold energy. The cross sections in Figs. 3-12 are plotted as functions of \sqrt{s} which equals or is larger than the threshold energy plus 5×10^{-4} GeV.

The reactions considered in the present work are all exothermic. When \sqrt{s} increases from threshold, the cross sections decrease rapidly, and then change slowly. In the slowly-changing region the cross sections may be tens of millibarns. For example, the cross sections for $p\psi(3770) \rightarrow \Sigma_c^{++} D^{*-}$, $p\psi(4040) \rightarrow \Lambda_c^+ \bar{D}^{*0}$, $p\psi(4160) \rightarrow \Sigma_c^{++} D^{*-}$, and $p\psi(4415) \rightarrow \Lambda_c^+ \bar{D}^{*0}$ can reach 20 mb, 30 mb, 21 mb, and 15 mb, respectively. According to the quantum numbers of $\psi(3770)$, $\psi(4040)$, $\psi(4160)$, and $\psi(4415)$ mesons, the numbers of their radial nodes are 0, 2, 1, and 3, respectively. If there is a node in the radial wave function $R_{L_B}(r_{c\bar{c}})$, cancellation between the wave functions on both sides of the node occurs in the integration involved in the transition amplitudes, thus cross sections are reduced. The $\psi(4040)$ mass is near the $\psi(4160)$ mass. Since the $\psi(4040)$ meson has one node more than the $\psi(4160)$ meson, the integration related to $\psi(4040)$ should have more cancellation than that related to $\psi(4160)$. However, the wave function of $\psi(4160)$ contains the spherical harmonics Y_{2M_B} ($M_B = -2, -1, 0, 1, 2$), and the wave function of $\psi(4040)$ contains the constant spherical harmonics Y_{00} . Then, the integration related to $\psi(4160)$ may have more cancellation than that related to $\psi(4040)$. Therefore, at the threshold energy plus 5×10^{-4} GeV, the cross sections for $p + \psi(4040)$ reactions are larger in Fig. 3 and Fig. 7 or smaller in Figs. 4-6 and Figs. 8-12 than the ones for $p + \psi(4160)$ reactions.

The mesonic quark-antiquark relative-motion wave functions are decreasing functions of the quark-antiquark relative momentum. $\phi_{A\text{space}}(\vec{p}_\rho, \vec{p}_\lambda)$ ($\phi_{C\text{space}}(\vec{p}'_\rho, \vec{p}'_\lambda)$) in the transition amplitudes is an exponentially decreasing function of \vec{p}_ρ and \vec{p}_λ (\vec{p}'_ρ and \vec{p}'_λ). The quark-antiquark relative momenta, \vec{p}_ρ , \vec{p}_λ , \vec{p}'_ρ , and \vec{p}'_λ , are given by the expressions enclosed by the parentheses that follow $\phi_{BJ_B J_{Bz}}$, $\phi_{D\text{rel}}$, $\phi_{A\text{space}}$, and $\phi_{C\text{space}}$ in Eqs. (30) and (31). These expressions may have $\vec{p}_{q_1 q_2 q_3, c\bar{c}}$ and $\vec{p}'_{q_1 q_2 c, q_3 \bar{c}}$. In the center-of-momentum frame of the proton and the charmonium, $\vec{p}_{q_1 q_2 q_3, c\bar{c}}$ and $\vec{p}'_{q_1 q_2 c, q_3 \bar{c}}$ equal \vec{P} and \vec{P}' , respectively. Therefore, the quark-antiquark relative momenta, \vec{p}_ρ , \vec{p}_λ , \vec{p}'_ρ , and \vec{p}'_λ , bear linear relation to \vec{P} and \vec{P}' . At the threshold energy plus 5×10^{-4} GeV, $|\vec{P}|$ almost equals zero, and $|\vec{P}'|$ of any $p + \psi(3770)$ reaction is smaller than $|\vec{P}'|$ of $p + \psi(4040)$, $p + \psi(4160)$, and $p + \psi(4415)$ reactions with the same final charmed baryon and the same final charmed meson in any of Figs. 3-12. The transition amplitudes for the $p + \psi(3770)$ reaction are larger than those for the $p + \psi(4040)$, $p + \psi(4160)$, and $p + \psi(4415)$ reactions. Therefore, at the threshold energy plus 5×10^{-4} GeV, the cross section for $p\psi(3770) \rightarrow \Lambda_c^+ \bar{D}^0$ in Fig. 3 is larger than those for $p\psi(4040) \rightarrow \Lambda_c^+ \bar{D}^0$, $p\psi(4160) \rightarrow \Lambda_c^+ \bar{D}^0$, and $p\psi(4415) \rightarrow \Lambda_c^+ \bar{D}^0$; similar results are displayed in Figs. 4-12. From the ten figures we can also understand that the cross sections for $p + \psi(4160)$ reactions at the threshold energy plus 5×10^{-4} GeV are larger than the ones for $p + \psi(4415)$ reactions.

The measured proton mass has a very small uncertainty, and the uncertainty is neglected here. The measured masses of charmed baryons have uncertainties [31], for example, the Λ_c^+ mass has an error of 0.14 MeV. The measured mass of every charmed baryon has a maximum and a minimum, for example, the Λ_c^+ mass has the maximum mass 2286.60 MeV and the minimum mass 2286.32 MeV. Fits to the maximum experimental masses of Λ_c^+ , Σ_c^{++} , Σ_c^+ , Σ_c^{*++} , and Σ_c^{*+} baryons give $\alpha_{\lambda_f} = 0.43$ GeV and

$$\alpha_\rho = 0.222571 \text{ GeV}, \quad m_{\Lambda_c^+} = 2.28660 \text{ GeV};$$

$$\alpha_\rho = 0.196254 \text{ GeV}, \quad m_{\Sigma_c^{++}} = 2.45411 \text{ GeV};$$

$$\alpha_\rho = 0.196365 \text{ GeV}, \quad m_{\Sigma_c^+} = 2.4533 \text{ GeV};$$

$$\alpha_\rho = 0.190894 \text{ GeV}, \quad m_{\Sigma_c^{*++}} = 2.51862 \text{ GeV};$$

$$\alpha_\rho = 0.19076 \text{ GeV}, \quad m_{\Sigma_c^{*+}} = 2.5198 \text{ GeV}.$$

Using these values of α_ρ and α_{λ_f} , we obtain unpolarized cross sections which are denoted as $\sigma_{\text{lm}}^{\text{unpol}}$. The differences between $\sigma_{\text{lm}}^{\text{unpol}}$ and σ^{unpol} shown in Figs. 3-12 are plotted as the lower solid, dashed, dotted, and dot-dashed curves in Figs. 13-22. Fits to the minimum experimental masses of Λ_c^+ , Σ_c^{++} , Σ_c^+ , Σ_c^{*++} , and Σ_c^{*+} baryons give $\alpha_{\lambda_f} = 0.43 \text{ GeV}$ and

$$\alpha_\rho = 0.222617 \text{ GeV}, \quad m_{\Lambda_c^+} = 2.28632 \text{ GeV};$$

$$\alpha_\rho = 0.196292 \text{ GeV}, \quad m_{\Sigma_c^{++}} = 2.45383 \text{ GeV};$$

$$\alpha_\rho = 0.196475 \text{ GeV}, \quad m_{\Sigma_c^+} = 2.4525 \text{ GeV};$$

$$\alpha_\rho = 0.190946 \text{ GeV}, \quad m_{\Sigma_c^{*++}} = 2.51822 \text{ GeV};$$

$$\alpha_\rho = 0.19136 \text{ GeV}, \quad m_{\Sigma_c^{*+}} = 2.5152 \text{ GeV}.$$

Using these values of α_ρ and α_{λ_f} , we obtain unpolarized cross sections which are denoted as $\sigma_{\text{sm}}^{\text{unpol}}$. The differences between $\sigma_{\text{sm}}^{\text{unpol}}$ and σ^{unpol} are plotted as the upper solid, dashed, dotted, and dot-dashed curves in Figs. 13-22. In every figure the orange (green, red, blue) band between the lower and upper solid (dashed, dotted, dot-dashed) curves show uncertainties of the unpolarized cross sections, which are labeled as σ_{uncer} and are caused by the uncertainties of the α_ρ value. However, the cross-section uncertainties are too small to be shown if the bands are attached to those curves in Figs. 3-12. The cross-section uncertainties are small because of the small uncertainties of the α_ρ values, which correspond to errors of measurement of the baryon masses.

In Refs. [1–3] $\psi(3770)$, $\psi(4040)$, $\psi(4160)$, and $\psi(4415)$ mesons are identified with the 1^3D_1 , 3^3S_1 , 2^3D_1 , and 4^3S_1 states of a charm quark and a charm antiquark. This identification is also true with the potential given in Eq. (33), and we then study inelastic scattering of a nucleon by the four $c\bar{c}$ mesons in the present work. However, we note that the quantum states of $\psi(3770)$ and $\psi(4415)$ mesons are open to debate. The 1^3D_1 $c\bar{c}$ state of the $\psi(3770)$ meson is suggested to be mixed with the 2^3S_1 $c\bar{c}$ state in Ref. [35], and may contain a four-quark component with the up- and down-quarks and antiquarks in Ref. [36]. The $\psi(4415)$ meson may be a 5^3S_1 $c\bar{c}$ state given in the screened potential

model [37], a 3^3D_1 $c\bar{c}$ state obtained with a quark potential derived from a Lagrangian with chiral symmetry breaking in Ref. [38], or a $c\bar{c}$ hybrid recognized in lattice calculations of meson masses [39], from the nonrelativistic reduction of the QCD Hamiltonian in the Coulomb gauge [40], and in the flux-tube model [41].

IV. SUMMARY

Flavor interchange between a nucleon and a $c\bar{c}$ meson breaks the meson. According to the quark interchange mechanism, we have derived formulas of the transition amplitudes that include wave functions and constituent-constituent potentials. The transition amplitudes are used to calculate unpolarized cross sections for the reactions: $pR \rightarrow \Lambda_c^+ \bar{D}^0$, $pR \rightarrow \Lambda_c^+ \bar{D}^{*0}$, $pR \rightarrow \Sigma_c^{++} D^-$, $pR \rightarrow \Sigma_c^{++} D^{*-}$, $pR \rightarrow \Sigma_c^+ \bar{D}^0$, $pR \rightarrow \Sigma_c^+ \bar{D}^{*0}$, $pR \rightarrow \Sigma_c^{*++} D^-$, $pR \rightarrow \Sigma_c^{*++} D^{*-}$, $pR \rightarrow \Sigma_c^{*+} \bar{D}^0$, and $pR \rightarrow \Sigma_c^{*+} \bar{D}^{*0}$, where R represents $\psi(3770)$, $\psi(4040)$, $\psi(4160)$, or $\psi(4415)$. These reactions are exothermic, and the \sqrt{s} dependence of their cross sections is so that the cross sections decrease rapidly near threshold and change slowly when the center-of-mass energy of the nucleon and the $c\bar{c}$ meson is not close to threshold. In the slowly-changing region the cross sections may be tens of millibarns. The cross sections also depend on nodes in the radial wave functions of the $c\bar{c}$ mesons. Numerical cross sections are parametrized. Cross sections for reactions of a neutron and a $c\bar{c}$ meson are obtained from those of a proton and the $c\bar{c}$ meson.

ACKNOWLEDGEMENTS

This work was supported by the project STRONG-2020 of European Center for Theoretical Studies in Nuclear Physics and Related Areas.

References

- [1] S. Godfrey and N. Isgur, Mesons in a relativized quark model with chromodynamics, Phys. Rev. D 32, 189 (1985).

- [2] T. Barnes, S. Godfrey, and E. S. Swanson, Higher charmonia, *Phys. Rev. D* 72, 054026 (2005).
- [3] J. Vijande, F. Fernández, and A. Valcarce, Constituent quark model study of the meson spectra, *J. Phys. G* 31, 481 (2005); P. G. Ortega, J. Segovia, D. R. Entem, and F. Fernández, Charmonium resonances in the 3.9 GeV/c² energy region and the $X(3915)/X(3930)$ puzzle, *Phys. Lett. B* 778, 1 (2018).
- [4] J. Siegrist *et al.*, Observation of a resonance at 4.4 GeV and additional structure near 4.1 GeV in e^+e^- annihilation, *Phys. Rev. Lett.* 36, 700 (1976); P. A. Rapidis *et al.*, Observation of a resonance in e^+e^- annihilation just above charm threshold, *Phys. Rev. Lett.* 39, 526 (1977).
- [5] R. H. Schindler *et al.*, Measurement of the parameters of the $\psi(3770)$ resonance, *Phys. Rev. D* 21, 2716 (1980).
- [6] R. Brandelik *et al.*, Total cross section for hadron production by e^+e^- annihilation at center of mass energies between 3.6 and 5.2 GeV, *Phys. Lett. B* 76, 361 (1978); R. Brandelik *et al.*, Results from DASP on e^+e^- annihilation between 3.1 and 5.2 GeV, *Z. Phys. C* 1, 233 (1979).
- [7] M. Ablikim *et al.*, Determination of the $\psi(3770)$, $\psi(4040)$, $\psi(4160)$ and $\psi(4415)$ resonance parameters, *Phys. Lett. B* 660, 315 (2008).
- [8] J. Z. Bai *et al.*, Evidence of $\psi(3770)$ non- $D\bar{D}$ decay to $J/\psi\pi^+\pi^-$, *Phys. Lett. B* 605, 63 (2005).
- [9] N. E. Adam *et al.*, Observation of $\psi(3770) \rightarrow \pi\pi J/\psi$ and measurement of $\Gamma_{ee}[\psi(2S)]$, *Phys. Rev. Lett.* 96, 082004 (2006).
- [10] T. E. Coan *et al.*, Charmonium decays of $Y(4260)$, $\psi(4160)$, and $\psi(4040)$, *Phys. Rev. Lett.* 96, 162003 (2006).
- [11] M. Ablikim *et al.*, Observation of $e^+e^- \rightarrow \eta J/\psi$ at center-of-mass energy $\sqrt{s} = 4.009$ GeV, *Phys. Rev. D* 86, 071101 (2012).

- [12] X. L. Wang *et al.*, Observation of $\psi(4040)$ and $\psi(4160)$ decay into $\eta J/\psi$, Phys. Rev. D 87, 051101 (2013).
- [13] Y. L. Han *et al.*, Measurement of $e^+e^- \rightarrow \gamma\chi_{cJ}$ via initial state radiation at Belle, Phys. Rev. D 92, 012011 (2015).
- [14] G. Pakhlova *et al.*, Observation of the $\psi(4415) \rightarrow D\bar{D}_2^*(2460)$ decay using initial-state radiation, Phys. Rev. Lett. 100, 062001 (2008).
- [15] B. Aubert *et al.*, Exclusive initial-state-radiation production of the $D\bar{D}$, $D^*\bar{D}$, and $D^*\bar{D}^*$ systems, Phys. Rev. D 79, 092001 (2009).
- [16] G. Pakhlova *et al.*, Measurement of the $e^+e^- \rightarrow D^0D^{*-}\pi^+$ cross section using initial-state radiation, Phys. Rev. D 80, 091101 (2009).
- [17] P. del Amo Sanchez *et al.*, Exclusive production of $D_s^+D_s^-$, $D_s^{*+}D_s^-$, and $D_s^{*+}D_s^{*-}$ via e^+e^- annihilation with initial-state radiation, Phys. Rev. D 82, 052004 (2010).
- [18] G. Pakhlova *et al.*, Measurement of $e^+e^- \rightarrow D_s^{(*)+}D_s^{(*)-}$ cross sections near threshold using initial-state radiation, Phys. Rev. D 83, 011101 (2011).
- [19] T. K. Pedlar *et al.*, Observation of the $h_c(1P)$ using e^+e^- collisions above the $D\bar{D}$ threshold, Phys. Rev. Lett. 107, 041803 (2011).
- [20] M. Ablikim *et al.*, Observation of $e^+e^- \rightarrow \omega\chi_{c1,2}$ near $\sqrt{s} = 4.42$ and 4.6 GeV, Phys. Rev. D 93, 011102 (2016).
- [21] M. Ablikim *et al.*, Measurement of cross sections for $e^+e^- \rightarrow \mu^+\mu^-$ at center-of-mass energies from 3.80 to 4.60 GeV, Phys. Rev. D 102, 112009 (2020).
- [22] M. Ablikim *et al.*, Measurement of the cross section for $e^+e^- \rightarrow \Lambda\bar{\Lambda}$ and evidence of the decay $\psi(3770) \rightarrow \Lambda\bar{\Lambda}$, Phys. Rev. D 104, L091104 (2021).
- [23] L.-K. Hao, K.-Y. Liu, and K.-T. Chao, D -wave charmonium production in e^+e^- annihilation at $\sqrt{s} = 10.6$ GeV, Phys. Lett. B 546, 216 (2002).

- [24] M. Piotrowska, F. Giacosa, and P. Kovacs, Can the $\psi(4040)$ explain the peak associated with $Y(4008)$, *Eur. Phys. J. C* 79, 98 (2019).
- [25] M. Bayar, N. Ikeno, and E. Oset, Analysis of the $\psi(4040)$ and $\psi(4160)$ decay into $D^{(*)}\bar{D}^{(*)}$, $D_s^{(*)}\bar{D}_s^{(*)}$, *Eur. Phys. J. C* 80, 222 (2020).
- [26] W.-X. Li, X.-M. Xu, and H. J. Weber, Cross sections for 2-to-1 meson-meson scattering, *Eur. Phys. J. C* 81, 225 (2021).
- [27] L.-Y. Li, X.-M. Xu, and H. J. Weber, Production of $\psi(4040)$, $\psi(4160)$, and $\psi(4415)$ mesons in hadronic matter, *Phys. Rev. D* 105, 114025 (2022).
- [28] F. Yuan, C.-F. Qiao, and K.-T. Chao, D -wave heavy quarkonium production in fixed target experiments, *Phys. Rev. D* 59, 014009 (1998).
- [29] W. Buchmüller and S.-H. H. Tye, Quarkonia and quantum chromodynamics, *Phys. Rev. D* 24, 132 (1981).
- [30] X.-M. Xu, J/ψ productions in nucleus-nucleus collisions at RHIC and LHC energies, *Nucl. Phys. A* 697, 825 (2002).
- [31] M. Tanabashi *et al.* (Particle Data Group), Review of particle physics: particle data groups, *Phys. Rev. D* 98, 030001 (2018) and 2019 update.
- [32] E. Colton, E. Malamud, P. E. Schlein, A. D. Johnson, V. J. Stenger, and P. G. Wohlmut, Measurement of $T = 2$ elastic $\pi\pi$ cross sections, *Phys. Rev. D* 3, 2028 (1971); N. B. Durusoy, M. Baubillier, R. George, M. Goldberg, A. M. Touchard, N. Armenise, M. T. Fogli-Muciaccia, and A. Silvestri, Study of the $I = 2$ $\pi\pi$ scattering from the reaction $\pi^-d \rightarrow \pi^-\pi^-p_s p$ at 9.0 GeV/c, *Phys. Lett.* 45 B, 517 (1973); M. J. Losty, V. Chaloupka, A. Ferrando, L. Montanet, E. Paul, D. Yaffe, A. Zieminski, J. Alitti, B. Gandois, and J. Louie, A study of $\pi^-\pi^-$ scattering from π^-p interactions at 3.93 GeV/c, *Nucl. Phys. B* 69, 185 (1974); W. Hoogland *et al.*, Measurement and analysis of the $\pi^+\pi^+$ system produced at small momentum transfer in the reaction $\pi^+p \rightarrow \pi^+\pi^+n$ at 12.5 GeV, *Nucl. Phys. B* 126, 109 (1977).

- [33] S. Capstick and N. Isgur, Baryons in a relativized quark model with chromodynamics, Phys. Rev. D 34, 2809 (1986).
- [34] J. P. Hilbert, N. Black, T. Barnes, and E. S. Swanson, Charmonium-nucleon dissociation cross sections in the quark model, Phys. Rev. C 75, 064907 (2007).
- [35] J. L. Rosner, Status of ψ'' decays to charmless final states, hep-ph/0405196; J. L. Rosner, ψ'' decays to charmless final states, Ann. Phys. (N.Y.) 319, 1 (2005).
- [36] M. B. Voloshin, $\bar{c}c$ purity of $\psi(3770)$ and ψ' challenged, Phys. Rev. D 71, 114003 (2005).
- [37] B.-Q. Li and K.-T. Chao, Higher charmonia and X , Y , Z states with screened potential, Phys. Rev. D 79, 094004 (2009).
- [38] J. Segovia, A. M. Yasser, D. R. Entem, and F. Fernández, $J^{PC} = 1^{--}$ hidden charm resonances, Phys. Rev. D 78, 114033 (2008).
- [39] C. W. Bernard, J. E. Hetrick, T. A. DeGrand, M. Wingate, C. DeTar, C. McNeile, S. Gottlieb, U. M. Heller, K. Rummukainen, B. Sugar, and D. Toussaint, Exotic mesons in quenched lattice QCD, Phys. Rev. D 56, 7039 (1997); Z. H. Mei and X. Q. Luo, Exotic mesons from quantum chromodynamics with improved gluon and quark actions on the anisotropic lattice, Int. J. Mod. Phys. A 18, 5713 (2003).
- [40] P. Guo, A. P. Szczepaniak, G. Galatà, A. Vassallo, and E. Santopinto, Heavy quarkonium hybrids from Coulomb gauge QCD, Phys. Rev. D 78, 056003 (2008).
- [41] N. Isgur, R. Kokoski, and J. Paton, Gluonic excitations of mesons: why they are missing and where to find them, Phys. Rev. Lett. 54, 869 (1985).

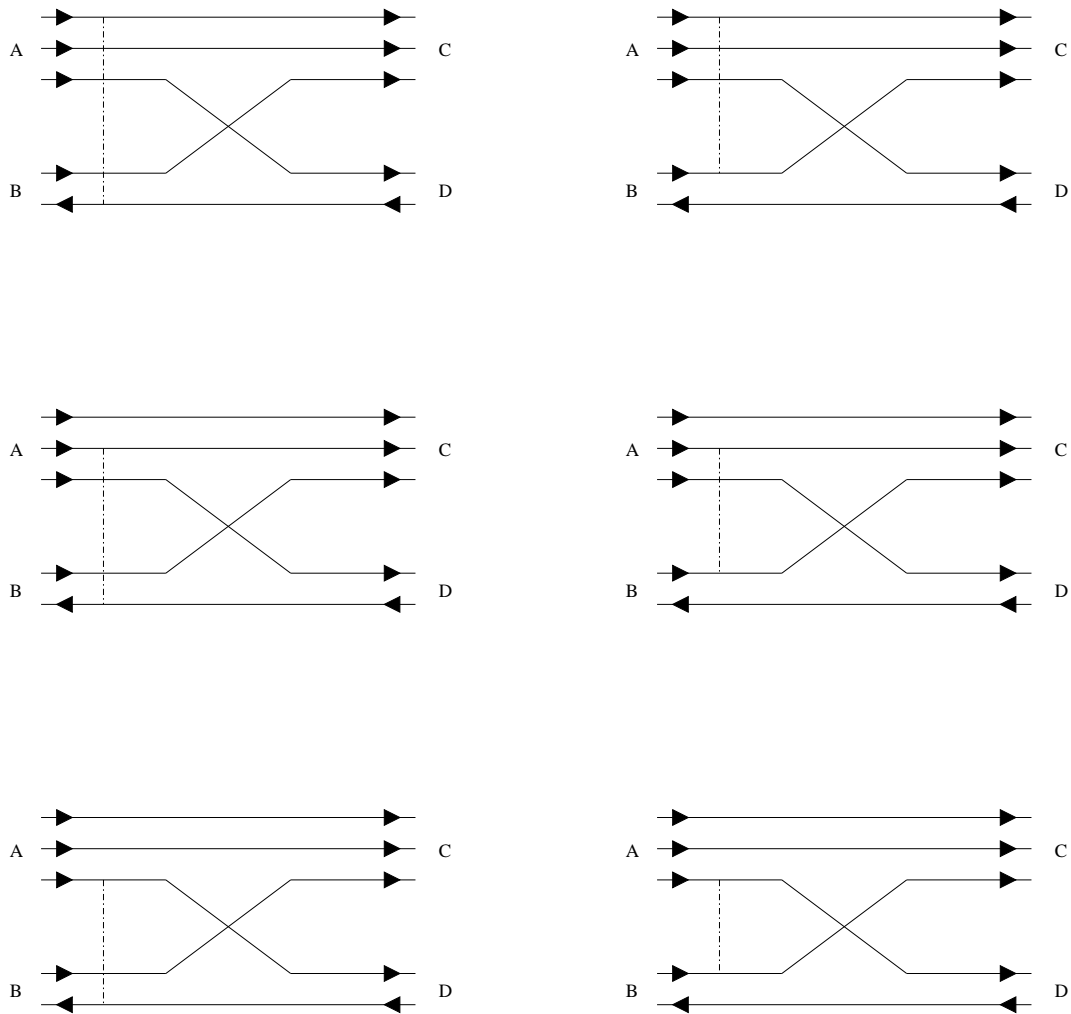


Figure 1: Scattering in the prior form. Solid lines with triangles right (left) represent quarks (antiquarks). Dot-dashed lines indicate interactions.

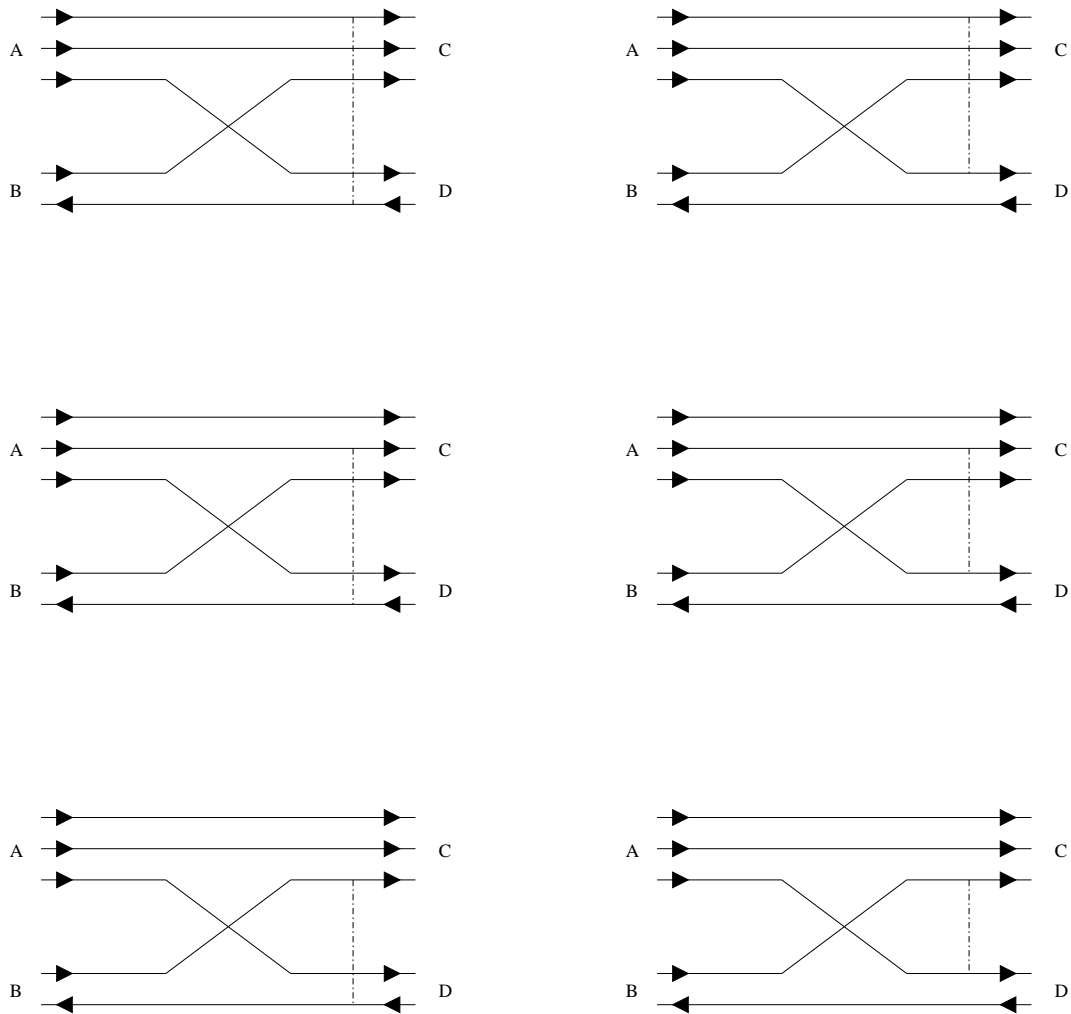


Figure 2: Scattering in the post form. Solid lines with triangles right (left) represent quarks (antiquarks). Dot-dashed lines indicate interactions.

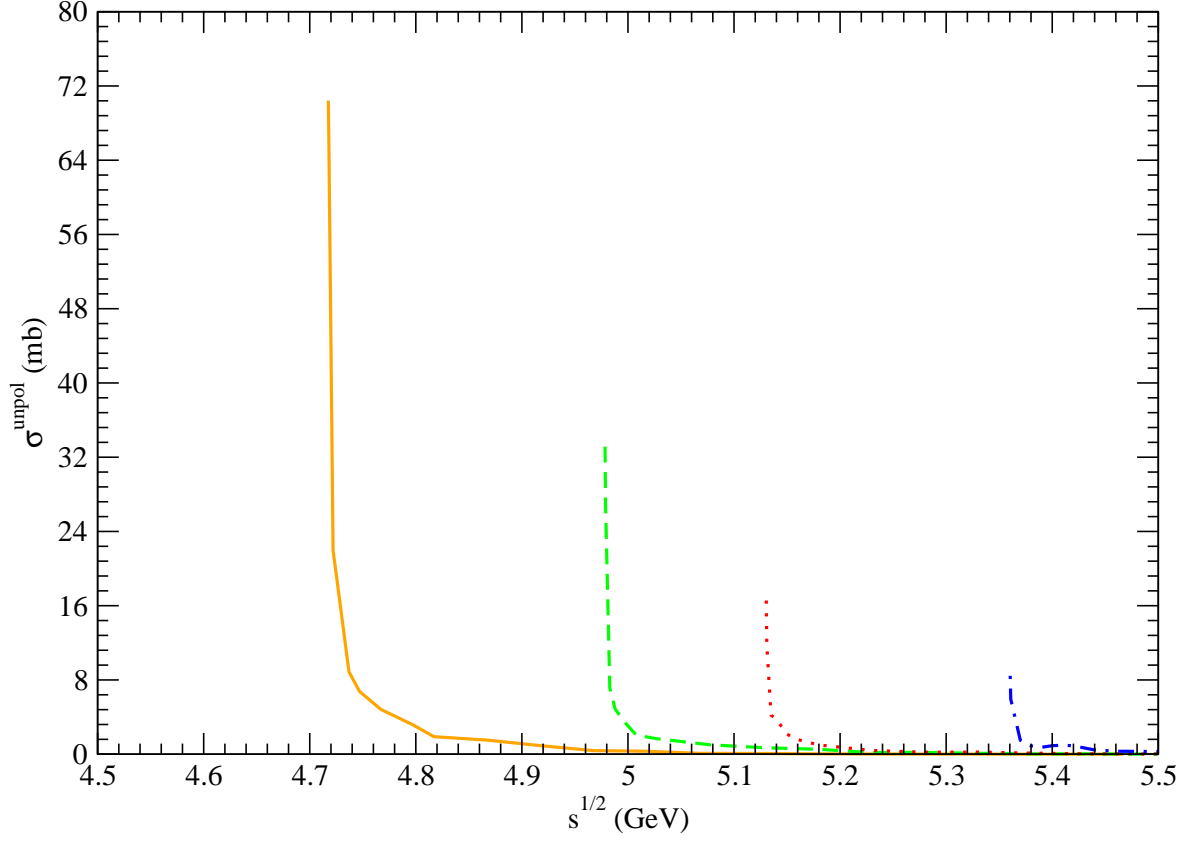


Figure 3: Solid, dashed, dotted, and dot-dashed curves stand for cross sections for $p\psi(3770) \rightarrow \Lambda_c^+ \bar{D}^0$, $p\psi(4040) \rightarrow \Lambda_c^+ \bar{D}^0$, $p\psi(4160) \rightarrow \Lambda_c^+ \bar{D}^0$, and $p\psi(4415) \rightarrow \Lambda_c^+ \bar{D}^0$, respectively.

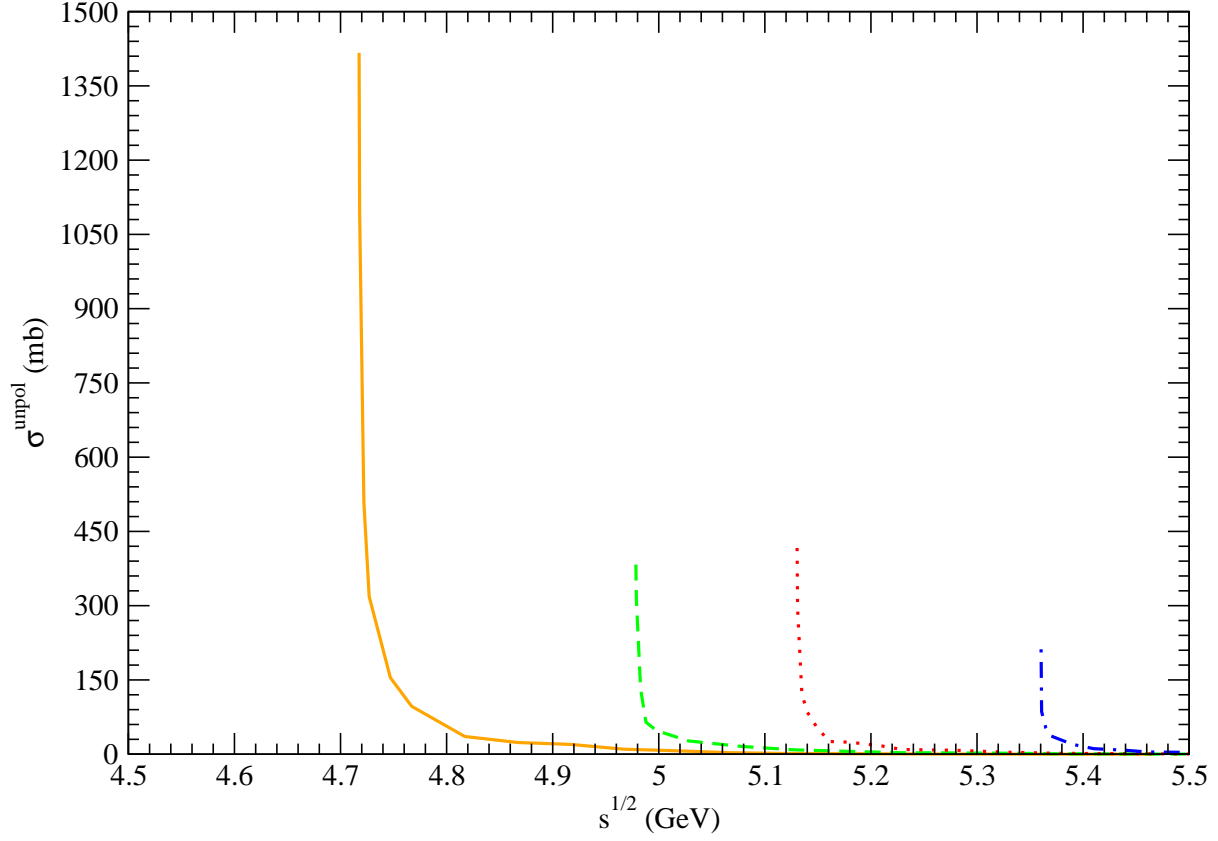


Figure 4: Solid, dashed, dotted, and dot-dashed curves stand for cross sections for $p\psi(3770) \rightarrow \Lambda_c^+ \bar{D}^{*0}$, $p\psi(4040) \rightarrow \Lambda_c^+ \bar{D}^{*0}$, $p\psi(4160) \rightarrow \Lambda_c^+ \bar{D}^{*0}$, and $p\psi(4415) \rightarrow \Lambda_c^+ \bar{D}^{*0}$, respectively.

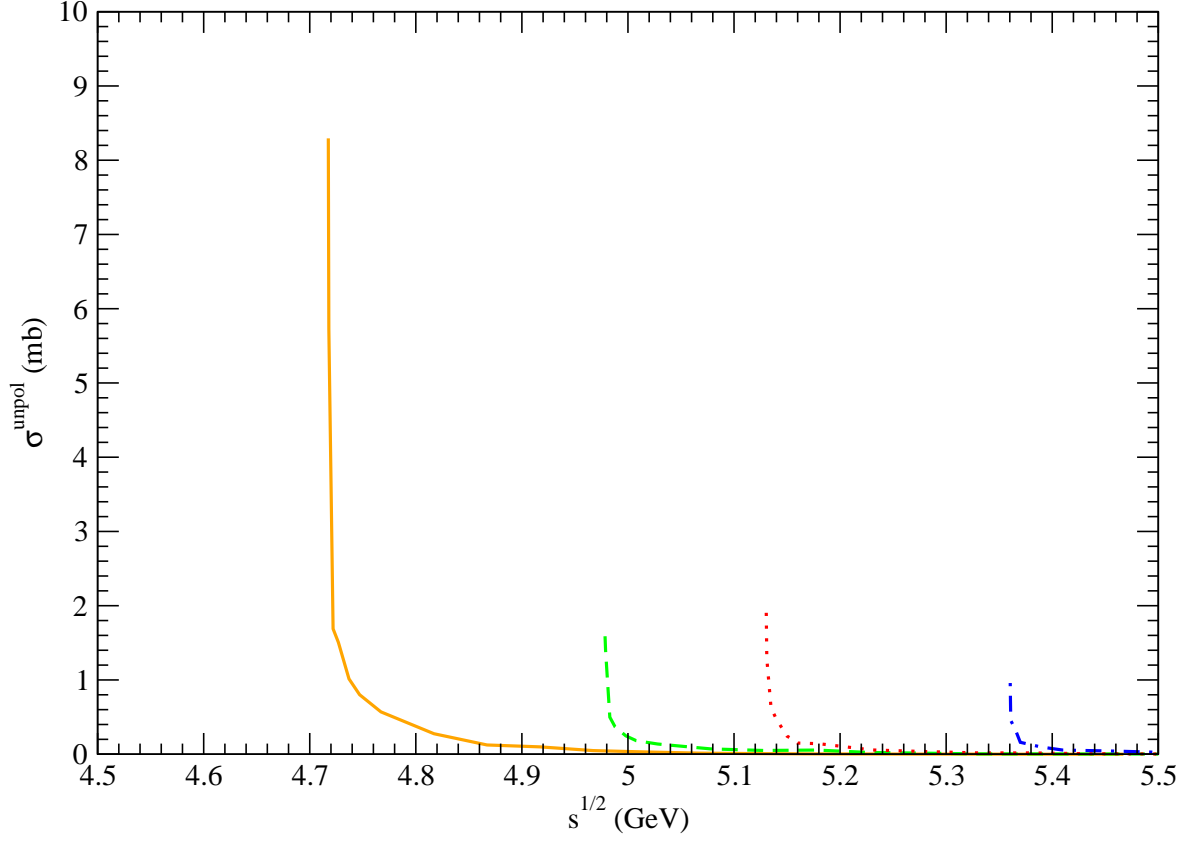


Figure 5: Solid, dashed, dotted, and dot-dashed curves stand for cross sections for $p\psi(3770) \rightarrow \Sigma_c^{++}D^-$, $p\psi(4040) \rightarrow \Sigma_c^{++}D^-$, $p\psi(4160) \rightarrow \Sigma_c^{++}D^-$, and $p\psi(4415) \rightarrow \Sigma_c^{++}D^-$, respectively.

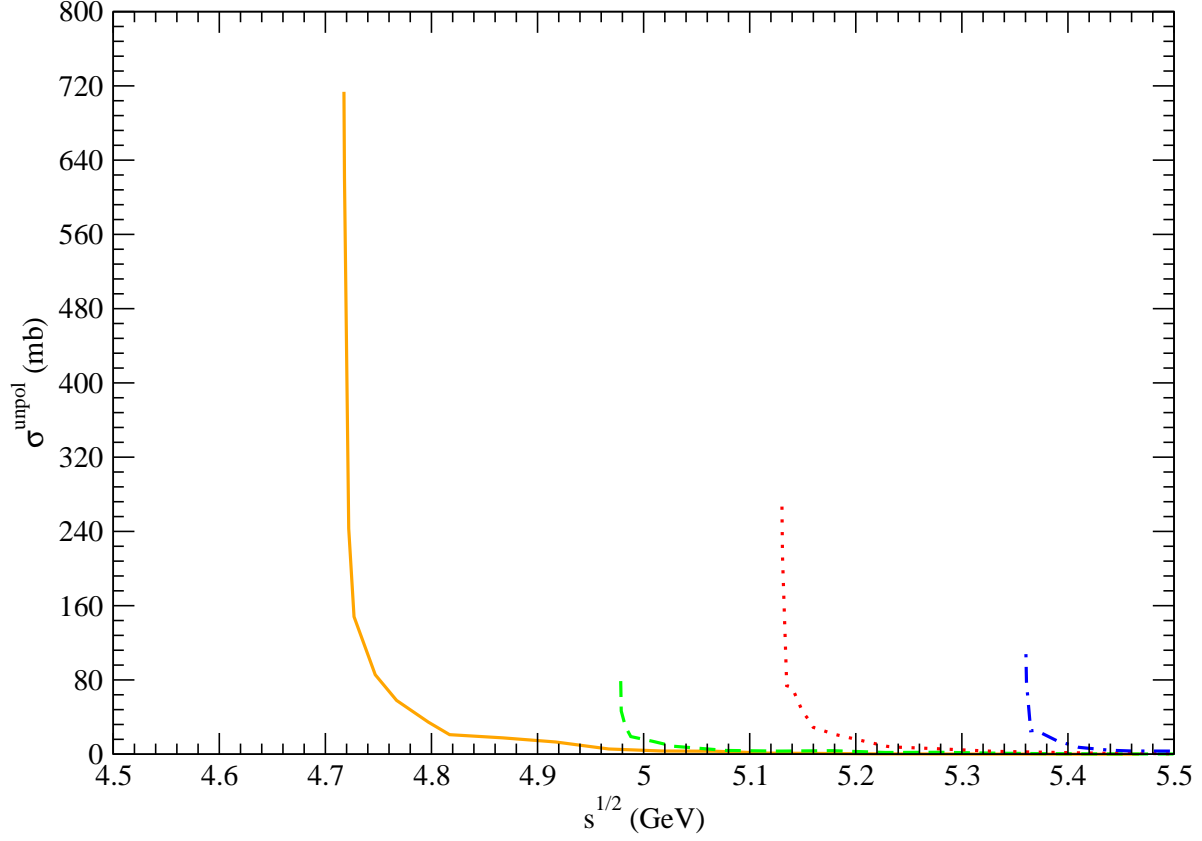


Figure 6: Solid, dashed, dotted, and dot-dashed curves stand for cross sections for $p\psi(3770) \rightarrow \Sigma_c^{++}D^{*-}$, $p\psi(4040) \rightarrow \Sigma_c^{++}D^{*-}$, $p\psi(4160) \rightarrow \Sigma_c^{++}D^{*-}$, and $p\psi(4415) \rightarrow \Sigma_c^{++}D^{*-}$, respectively.

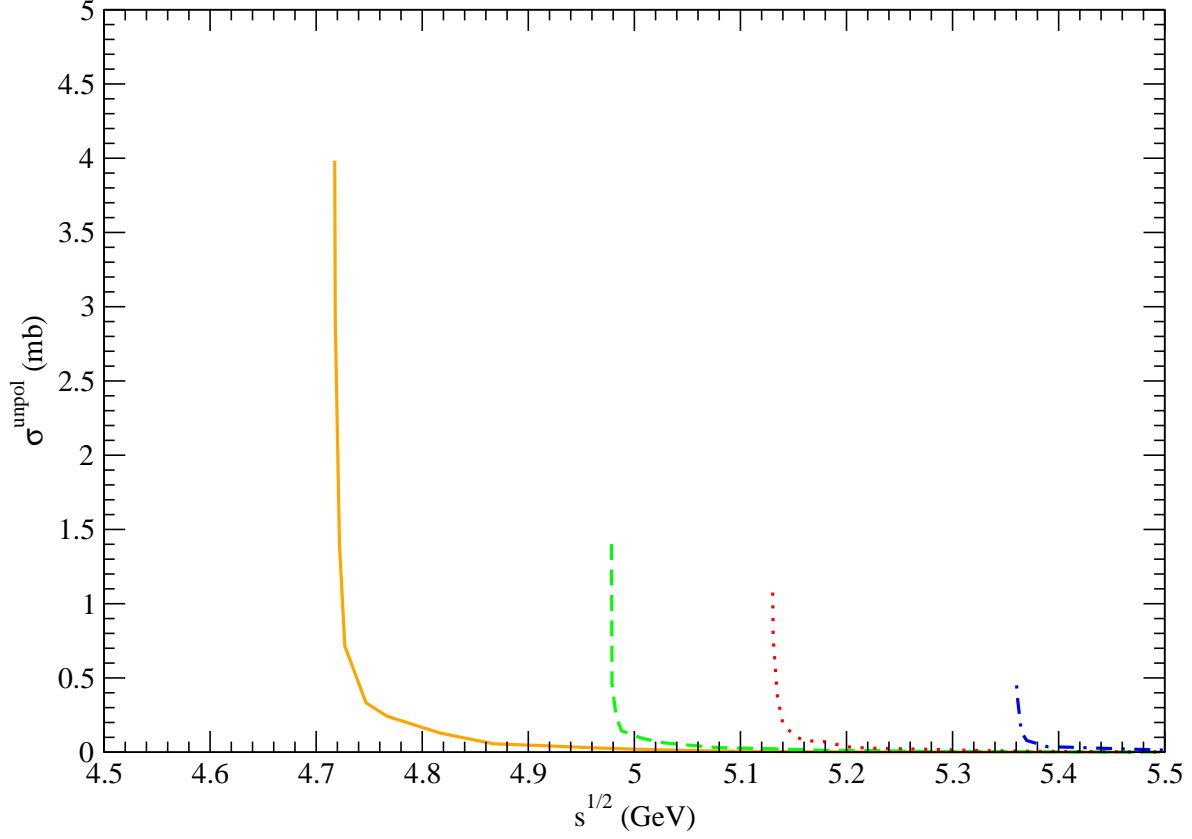


Figure 7: Solid, dashed, dotted, and dot-dashed curves stand for cross sections for $p\psi(3770) \rightarrow \Sigma_c^+ \bar{D}^0$, $p\psi(4040) \rightarrow \Sigma_c^+ \bar{D}^0$, $p\psi(4160) \rightarrow \Sigma_c^+ \bar{D}^0$, and $p\psi(4415) \rightarrow \Sigma_c^+ \bar{D}^0$, respectively.

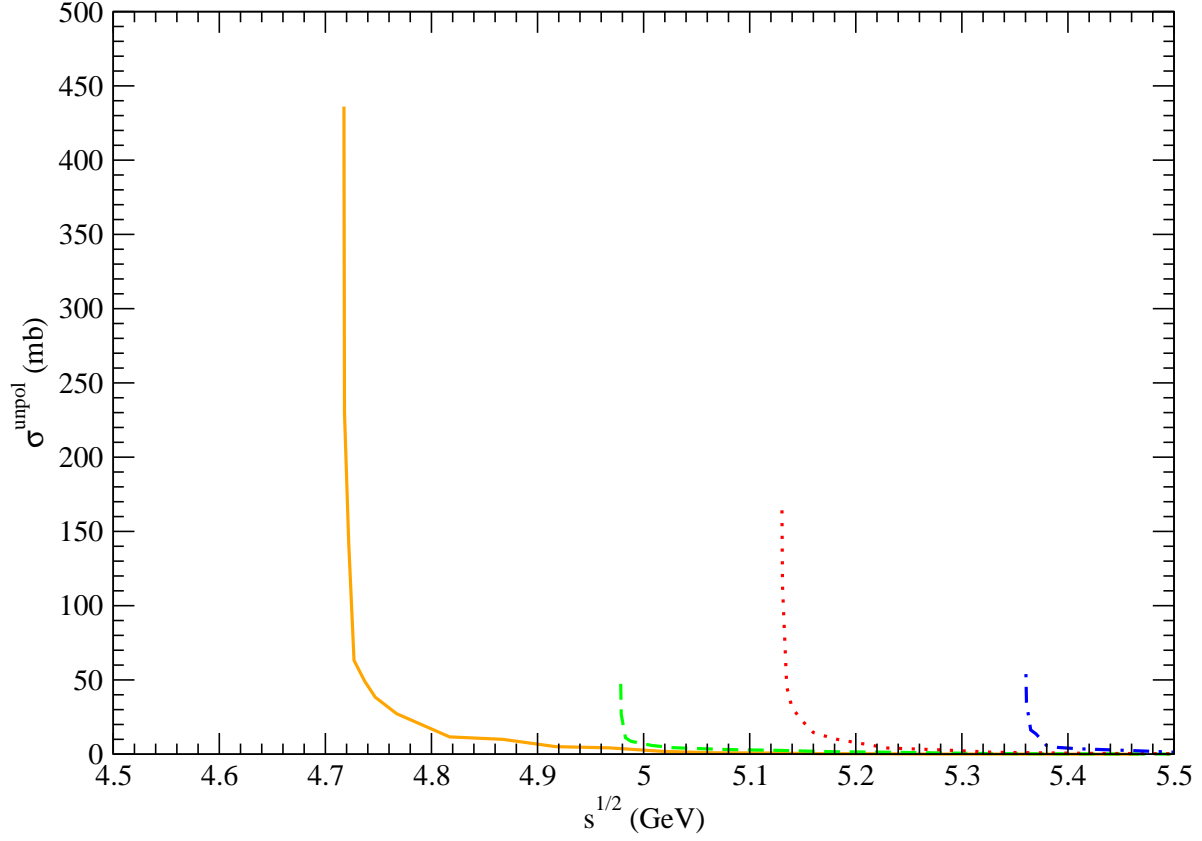


Figure 8: Solid, dashed, dotted, and dot-dashed curves stand for cross sections for $p\psi(3770) \rightarrow \Sigma_c^+ \bar{D}^{*0}$, $p\psi(4040) \rightarrow \Sigma_c^+ \bar{D}^{*0}$, $p\psi(4160) \rightarrow \Sigma_c^+ \bar{D}^{*0}$, and $p\psi(4415) \rightarrow \Sigma_c^+ \bar{D}^{*0}$, respectively.

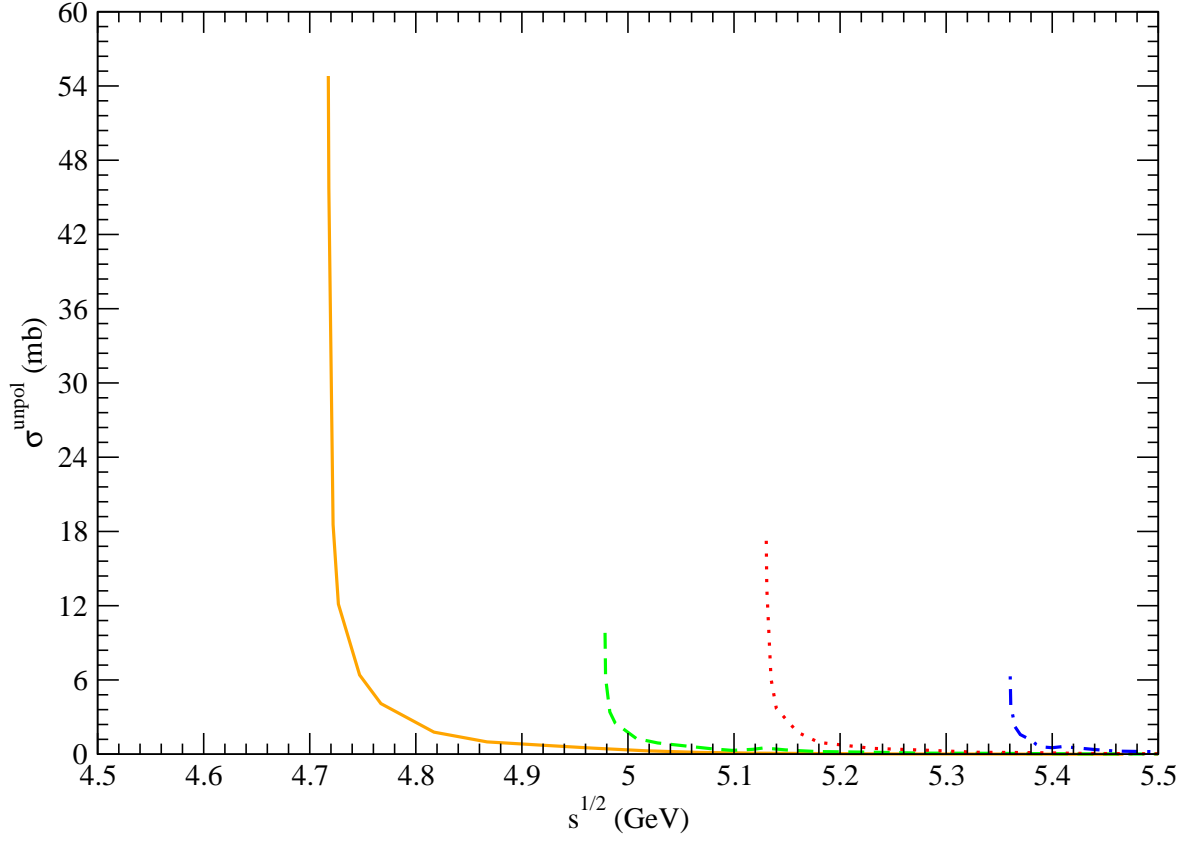


Figure 9: Solid, dashed, dotted, and dot-dashed curves stand for cross sections for $p\psi(3770) \rightarrow \Sigma_c^{*++}D^-$, $p\psi(4040) \rightarrow \Sigma_c^{*++}D^-$, $p\psi(4160) \rightarrow \Sigma_c^{*++}D^-$, and $p\psi(4415) \rightarrow \Sigma_c^{*++}D^-$, respectively.

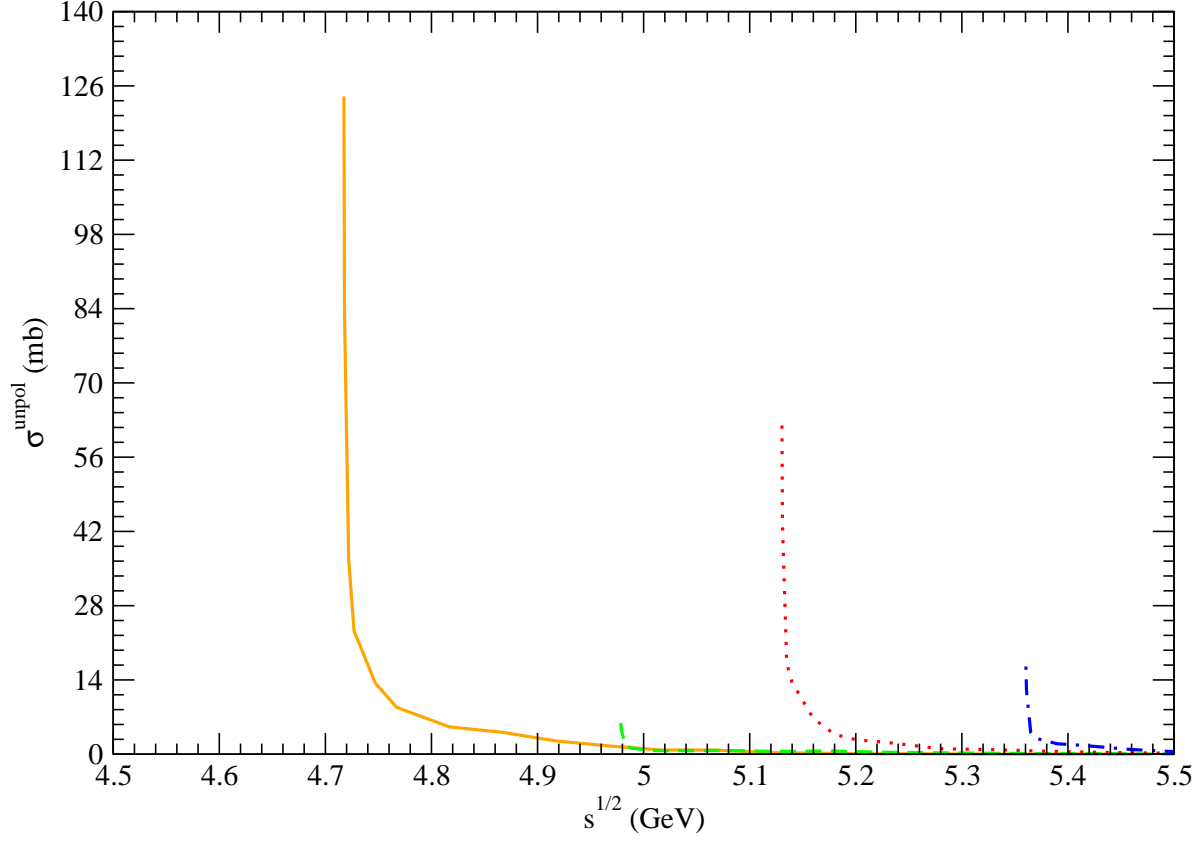


Figure 10: Solid, dashed, dotted, and dot-dashed curves stand for cross sections for $p\psi(3770) \rightarrow \Sigma_c^{*++}D^{*-}$, $p\psi(4040) \rightarrow \Sigma_c^{*++}D^{*-}$, $p\psi(4160) \rightarrow \Sigma_c^{*++}D^{*-}$, and $p\psi(4415) \rightarrow \Sigma_c^{*++}D^{*-}$, respectively.

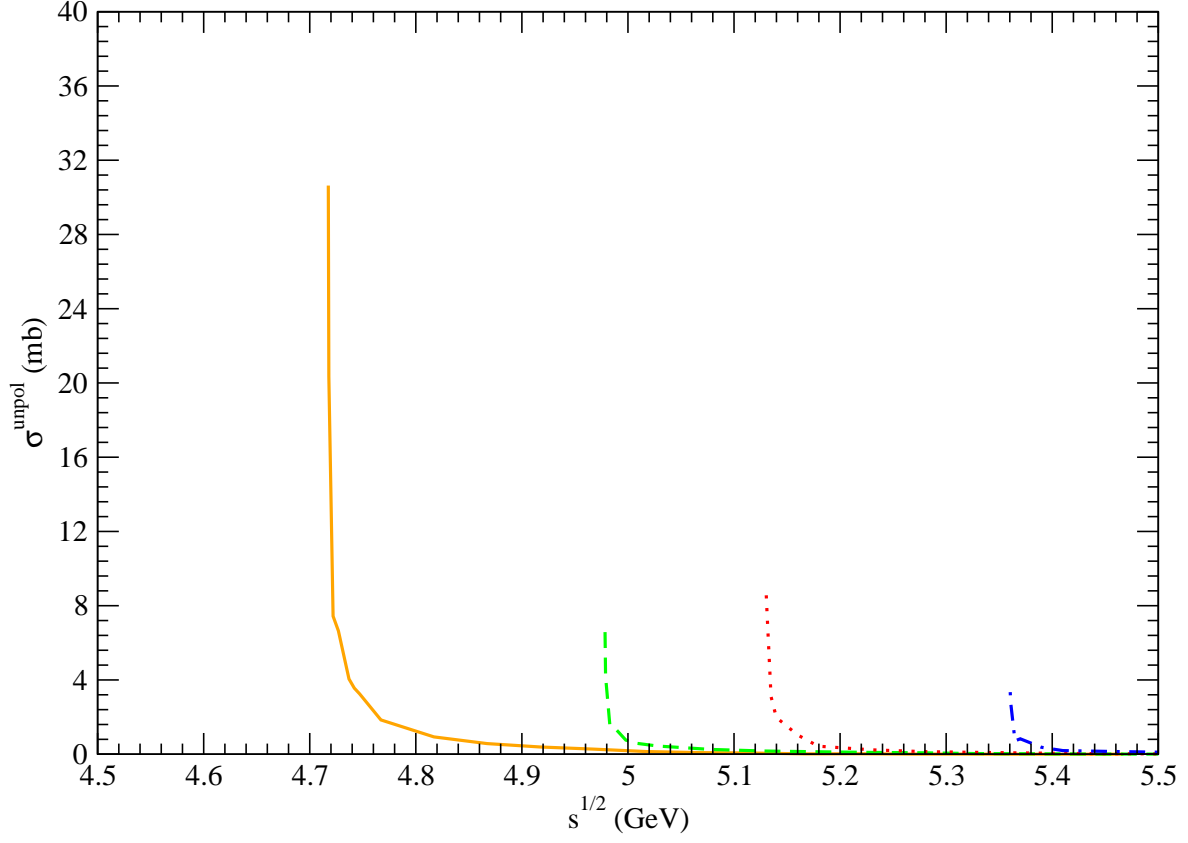


Figure 11: Solid, dashed, dotted, and dot-dashed curves stand for cross sections for $p\psi(3770) \rightarrow \Sigma_c^{*+} \bar{D}^0$, $p\psi(4040) \rightarrow \Sigma_c^{*+} \bar{D}^0$, $p\psi(4160) \rightarrow \Sigma_c^{*+} \bar{D}^0$, and $p\psi(4415) \rightarrow \Sigma_c^{*+} \bar{D}^0$, respectively.

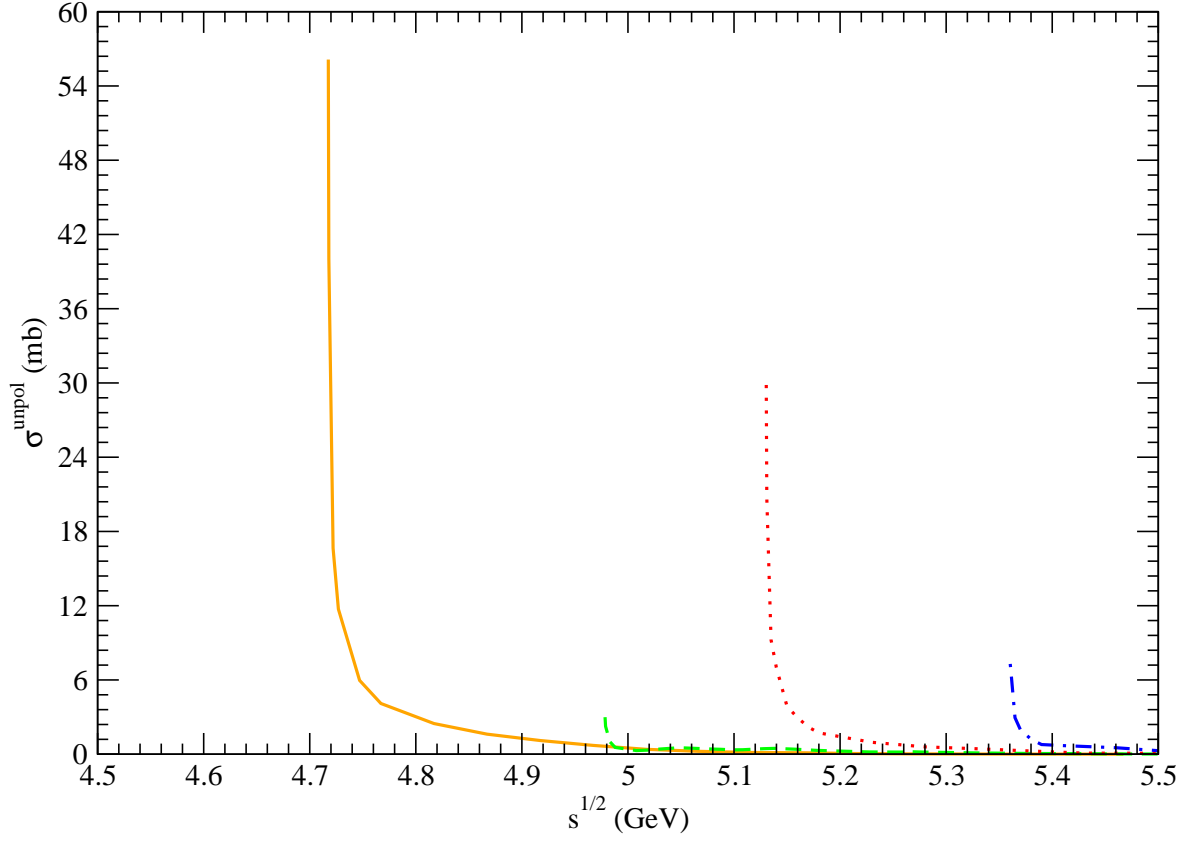


Figure 12: Solid, dashed, dotted, and dot-dashed curves stand for cross sections for $p\psi(3770) \rightarrow \Sigma_c^{*+} \bar{D}^{*0}$, $p\psi(4040) \rightarrow \Sigma_c^{*+} \bar{D}^{*0}$, $p\psi(4160) \rightarrow \Sigma_c^{*+} \bar{D}^{*0}$, and $p\psi(4415) \rightarrow \Sigma_c^{*+} \bar{D}^{*0}$, respectively.

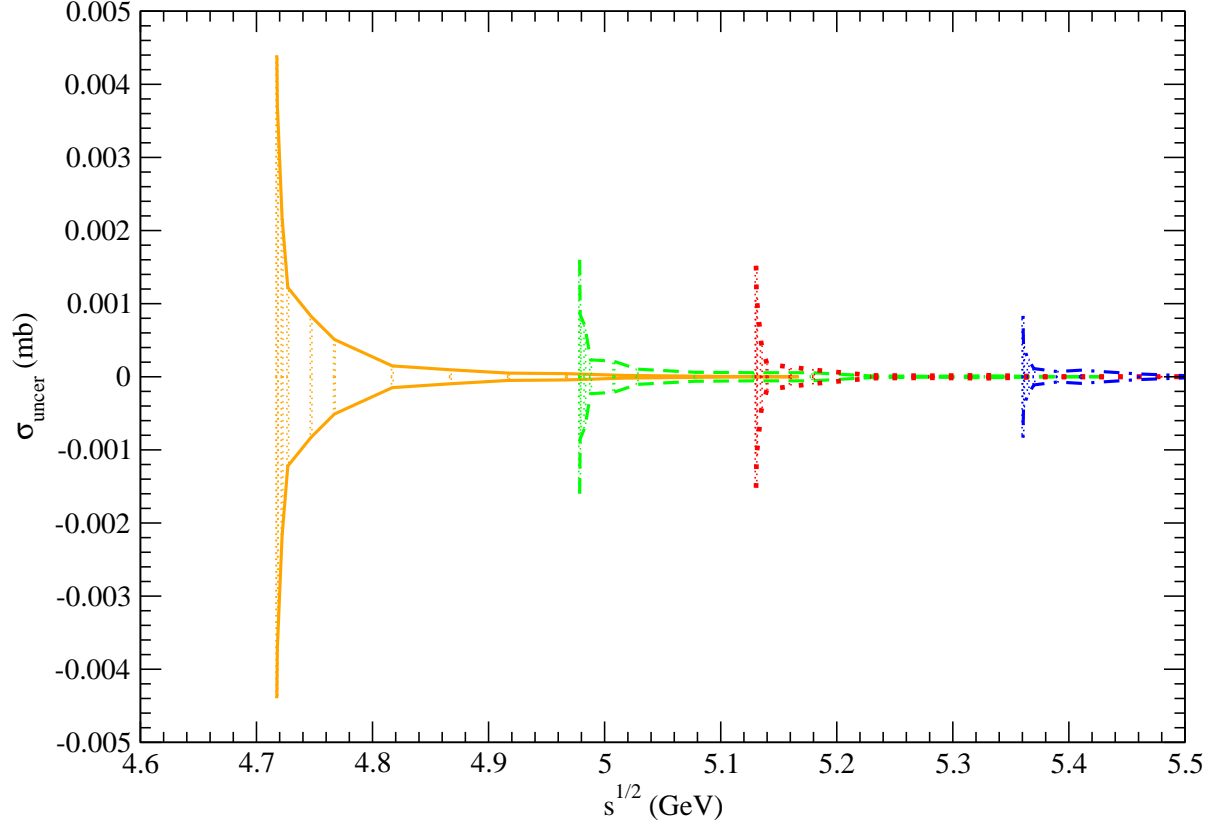


Figure 13: The error band between the two solid (dashed, dotted, and dot-dashed) curves indicates uncertainties of the unpolarized cross sections for $p\psi(3770) \rightarrow \Lambda_c^+ \bar{D}^0$ ($p\psi(4040) \rightarrow \Lambda_c^+ \bar{D}^0$, $p\psi(4160) \rightarrow \Lambda_c^+ \bar{D}^0$, and $p\psi(4415) \rightarrow \Lambda_c^+ \bar{D}^0$).

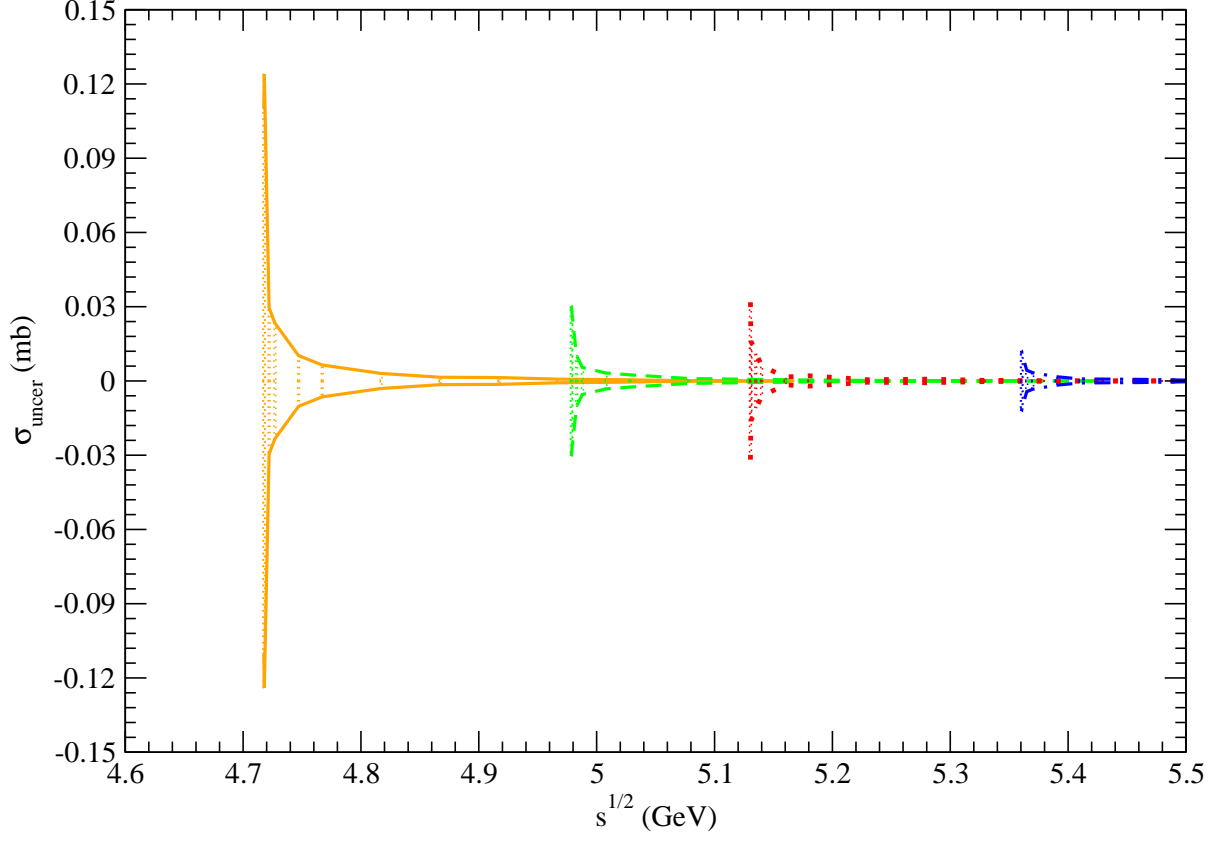


Figure 14: The error band between the two solid (dashed, dotted, and dot-dashed) curves indicates uncertainties of the unpolarized cross sections for $p\psi(3770) \rightarrow \Lambda_c^+ \bar{D}^{*0}$ ($p\psi(4040) \rightarrow \Lambda_c^+ \bar{D}^{*0}$, $p\psi(4160) \rightarrow \Lambda_c^+ \bar{D}^{*0}$, and $p\psi(4415) \rightarrow \Lambda_c^+ \bar{D}^{*0}$).

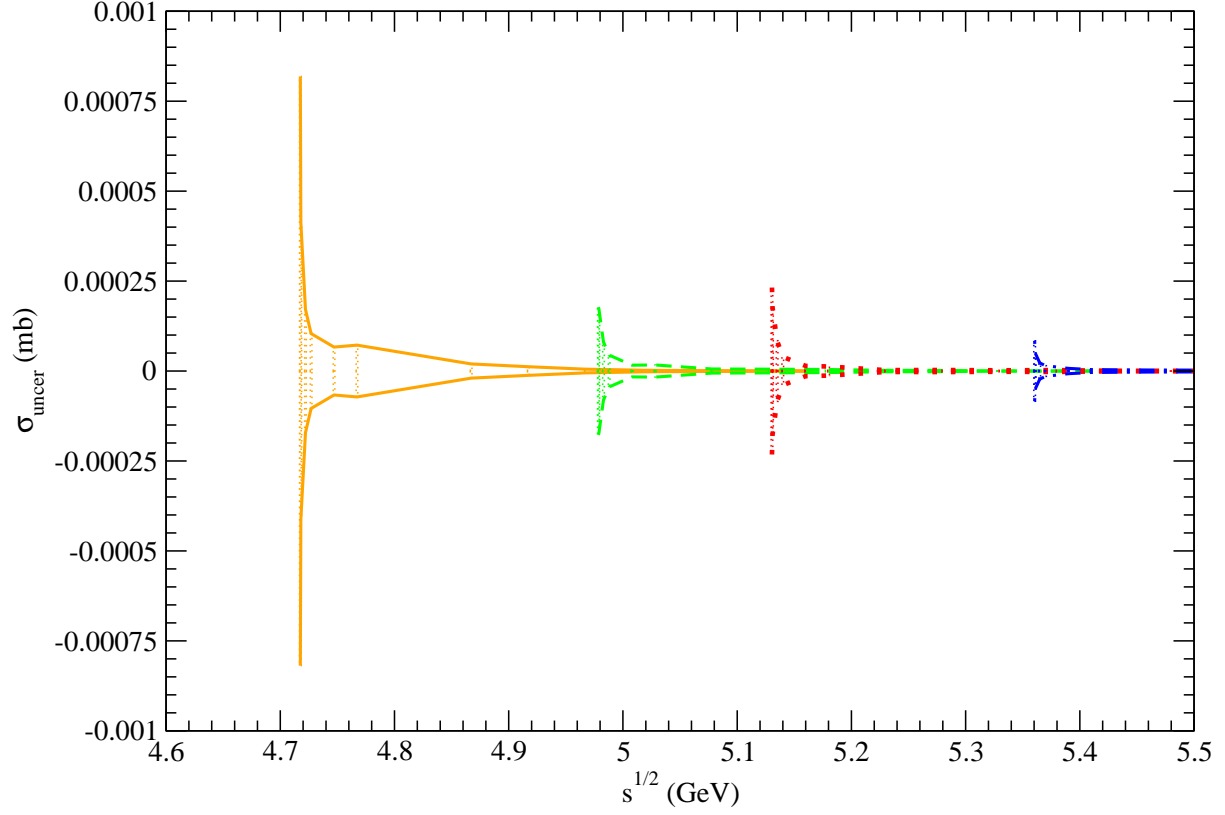


Figure 15: The error band between the two solid (dashed, dotted, and dot-dashed) curves indicates uncertainties of the unpolarized cross sections for $p\psi(3770) \rightarrow \Sigma_c^{++}D^-$ ($p\psi(4040) \rightarrow \Sigma_c^{++}D^-$, $p\psi(4160) \rightarrow \Sigma_c^{++}D^-$, and $p\psi(4415) \rightarrow \Sigma_c^{++}D^-$).

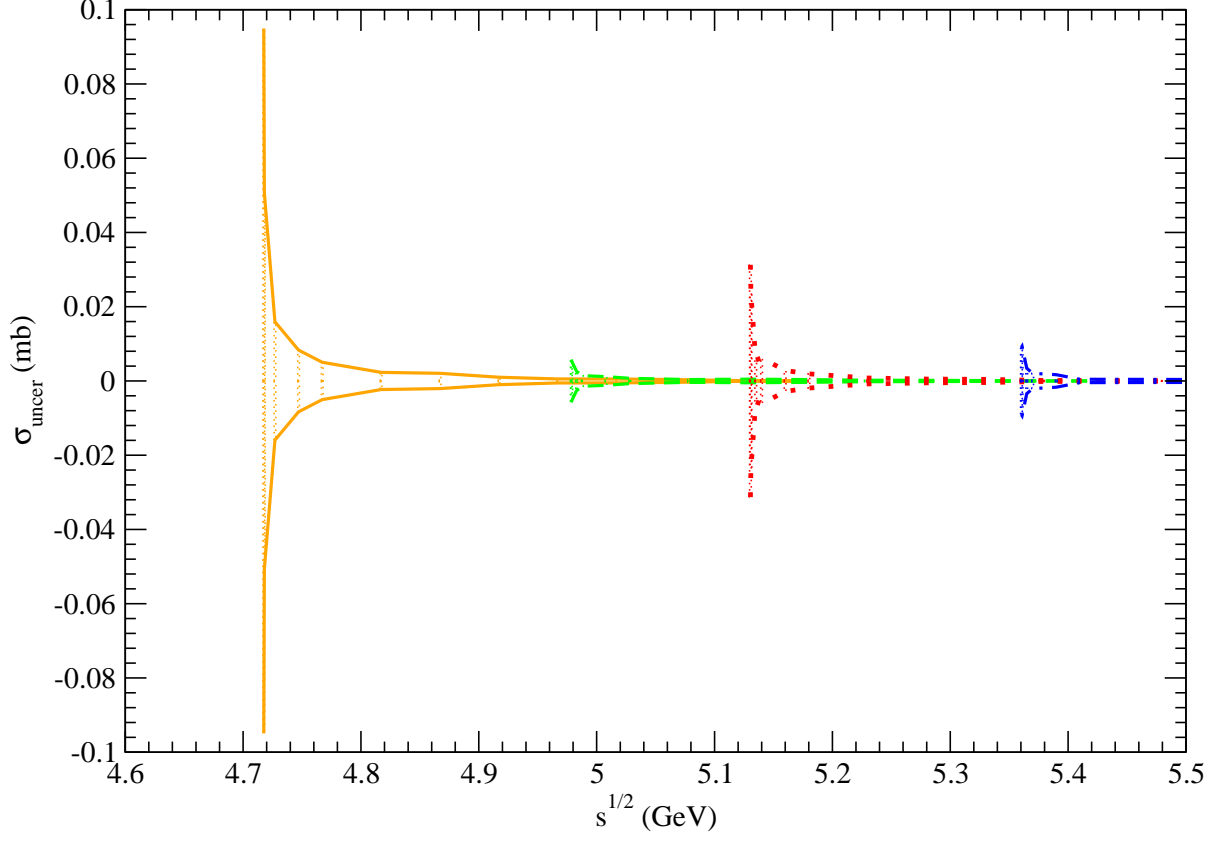


Figure 16: The error band between the two solid (dashed, dotted, and dot-dashed) curves indicates uncertainties of the unpolarized cross sections for $p\psi(3770) \rightarrow \Sigma_c^{++}D^{*-}$ ($p\psi(4040) \rightarrow \Sigma_c^{++}D^{*-}$, $p\psi(4160) \rightarrow \Sigma_c^{++}D^{*-}$, and $p\psi(4415) \rightarrow \Sigma_c^{++}D^{*-}$).

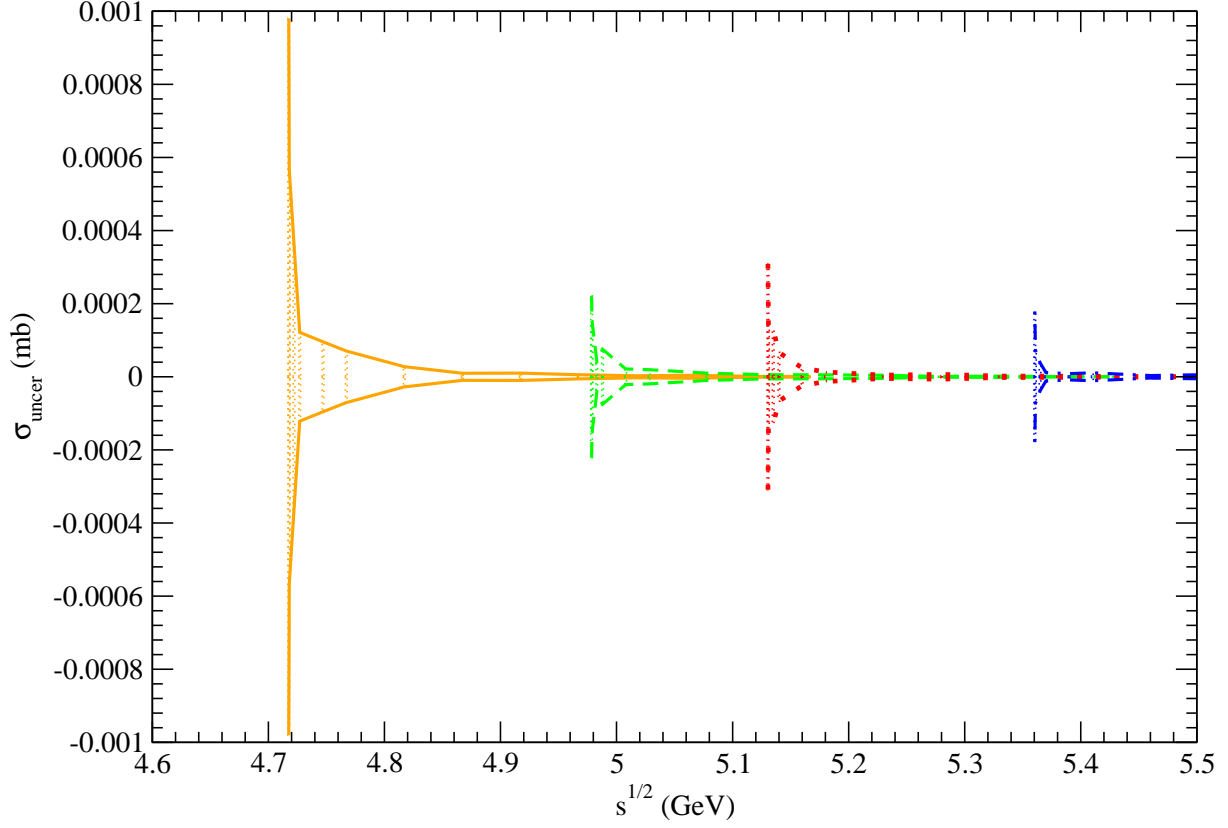


Figure 17: The error band between the two solid (dashed, dotted, and dot-dashed) curves indicates uncertainties of the unpolarized cross sections for $p\psi(3770) \rightarrow \Sigma_c^+ \bar{D}^0$ ($p\psi(4040) \rightarrow \Sigma_c^+ \bar{D}^0$, $p\psi(4160) \rightarrow \Sigma_c^+ \bar{D}^0$, and $p\psi(4415) \rightarrow \Sigma_c^+ \bar{D}^0$).

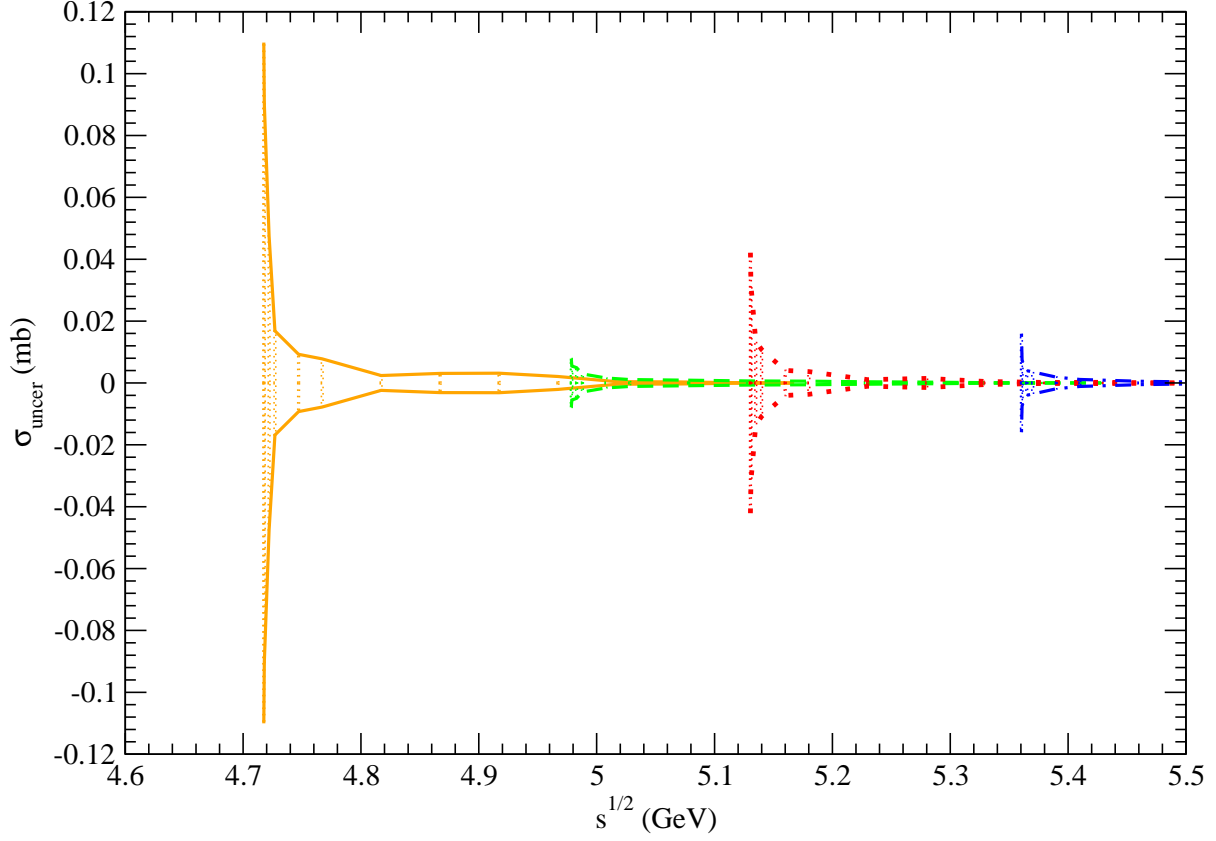


Figure 18: The error band between the two solid (dashed, dotted, and dot-dashed) curves indicates uncertainties of the unpolarized cross sections for $p\psi(3770) \rightarrow \Sigma_c^+ \bar{D}^{*0}$ ($p\psi(4040) \rightarrow \Sigma_c^+ \bar{D}^{*0}$, $p\psi(4160) \rightarrow \Sigma_c^+ \bar{D}^{*0}$, and $p\psi(4415) \rightarrow \Sigma_c^+ \bar{D}^{*0}$).

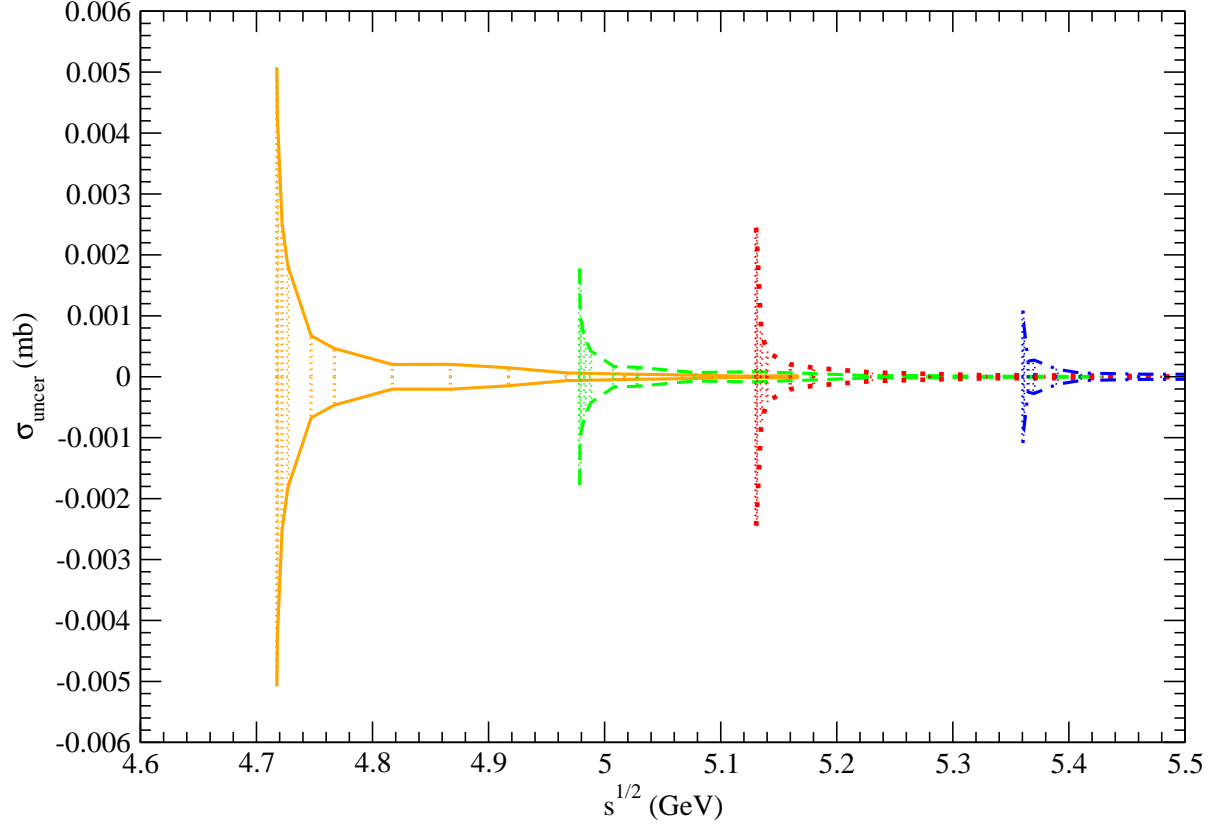


Figure 19: The error band between the two solid (dashed, dotted, and dot-dashed) curves indicates uncertainties of the unpolarized cross sections for $p\psi(3770) \rightarrow \Sigma_c^{*++}D^-$ ($p\psi(4040) \rightarrow \Sigma_c^{*++}D^-$, $p\psi(4160) \rightarrow \Sigma_c^{*++}D^-$, and $p\psi(4415) \rightarrow \Sigma_c^{*++}D^-$).

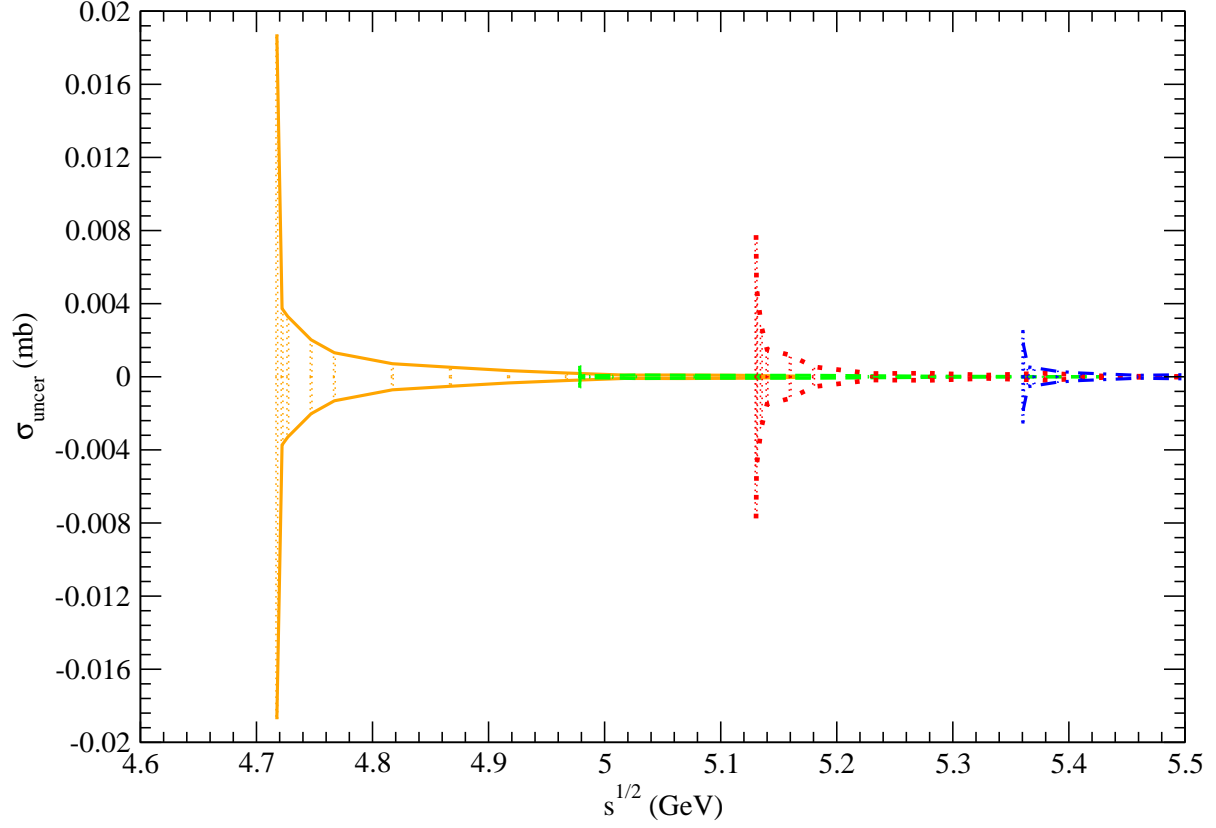


Figure 20: The error band between the two solid (dashed, dotted, and dot-dashed) curves indicates uncertainties of the unpolarized cross sections for $p\psi(3770) \rightarrow \Sigma_c^{*++}D^{*-}$ ($p\psi(4040) \rightarrow \Sigma_c^{*++}D^{*-}$, $p\psi(4160) \rightarrow \Sigma_c^{*++}D^{*-}$, and $p\psi(4415) \rightarrow \Sigma_c^{*++}D^{*-}$).

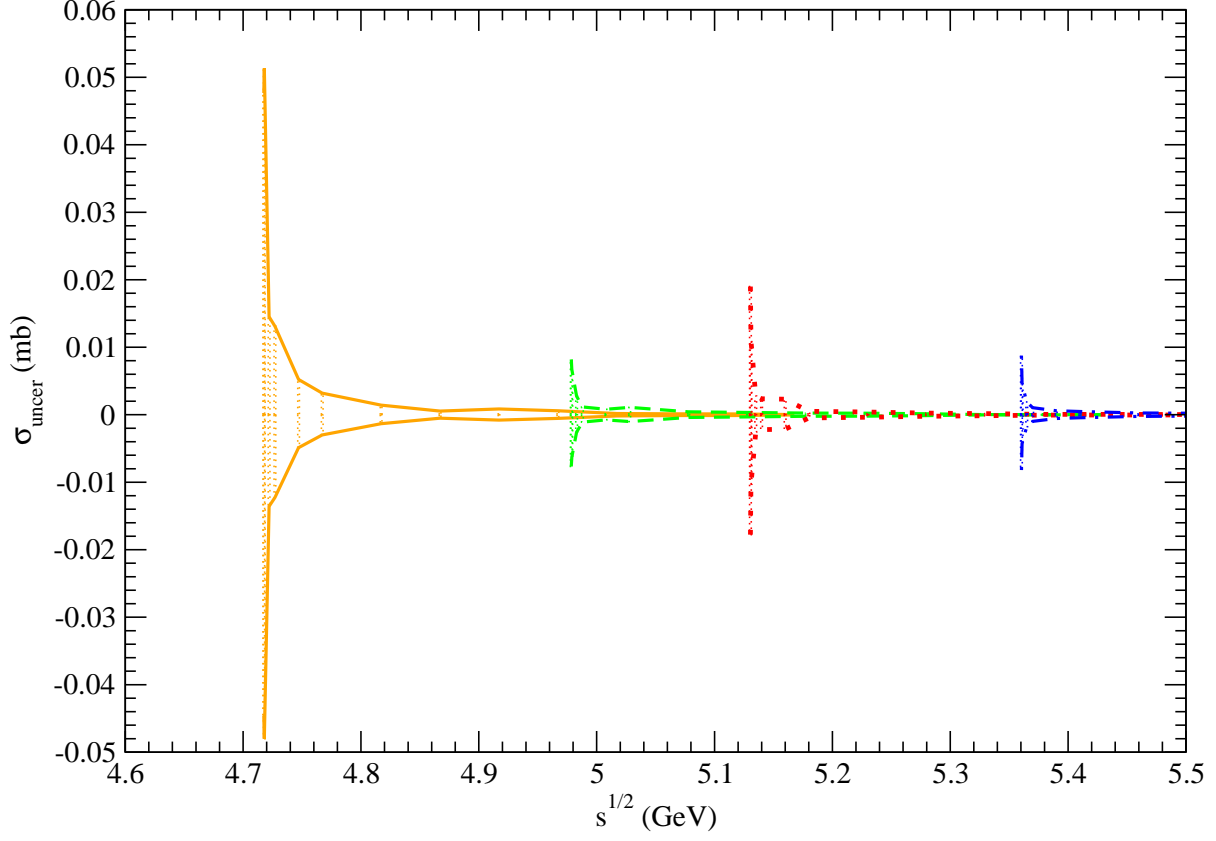


Figure 21: The error band between the two solid (dashed, dotted, and dot-dashed) curves indicates uncertainties of the unpolarized cross sections for $p\psi(3770) \rightarrow \Sigma_c^{*+} \bar{D}^0$ ($p\psi(4040) \rightarrow \Sigma_c^{*+} \bar{D}^0$, $p\psi(4160) \rightarrow \Sigma_c^{*+} \bar{D}^0$, and $p\psi(4415) \rightarrow \Sigma_c^{*+} \bar{D}^0$).

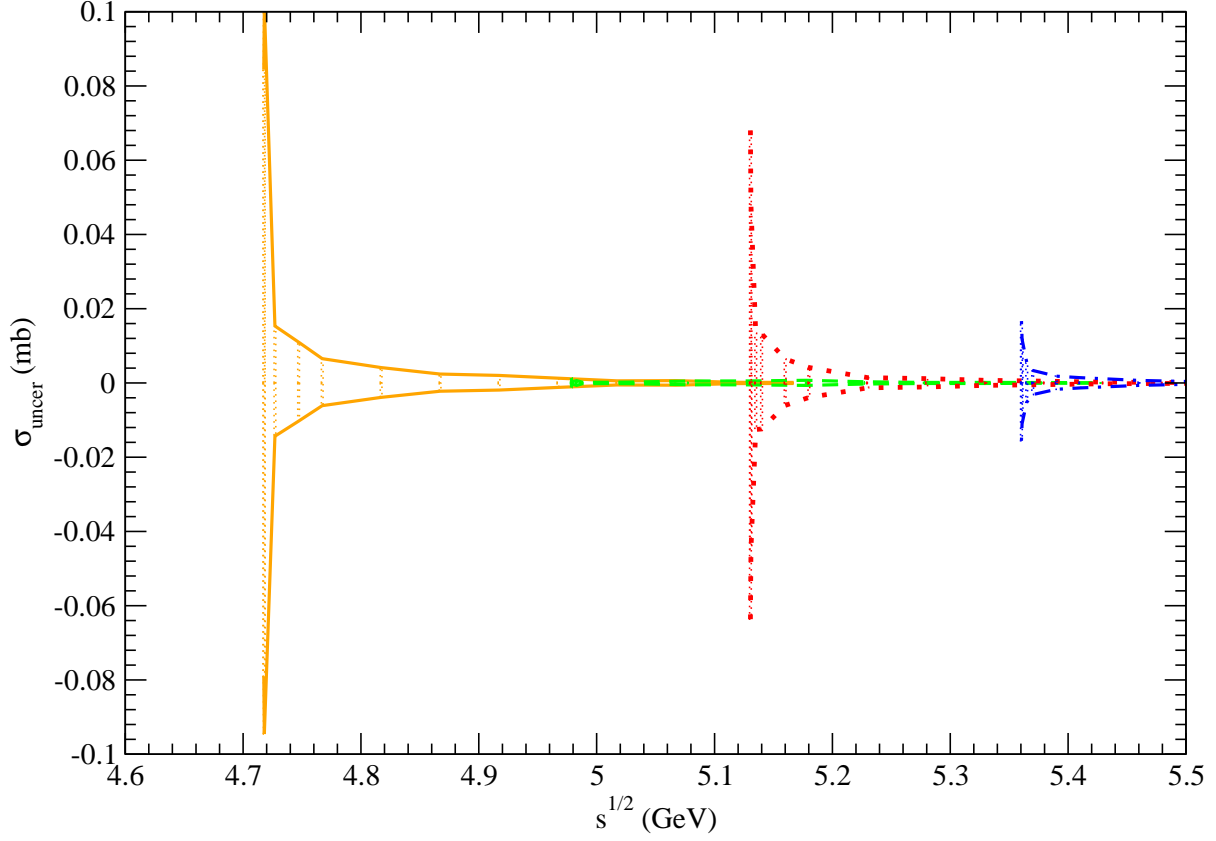


Figure 22: The error band between the two solid (dashed, dotted, and dot-dashed) curves indicates uncertainties of the unpolarized cross sections for $p\psi(3770) \rightarrow \Sigma_c^{*+} \bar{D}^{*0}$ ($p\psi(4040) \rightarrow \Sigma_c^{*+} \bar{D}^{*0}$, $p\psi(4160) \rightarrow \Sigma_c^{*+} \bar{D}^{*0}$, and $p\psi(4415) \rightarrow \Sigma_c^{*+} \bar{D}^{*0}$).

Table 1: Values of the parameters. a_1 and a_2 are in units of millibarns; b_1 and b_2 are in units of GeV; c_1 and c_2 are dimensionless.

reaction	a_1	b_1	c_1	a_2	b_2	c_2
$p\psi(3770) \rightarrow \Lambda_c^+ \bar{D}^0$	0.13	0.01	0.51	0.23	0.09	1.08
$p\psi(4040) \rightarrow \Lambda_c^+ \bar{D}^0$	0.065	0.068	0.41	0.017	0.18	62.4
$p\psi(4160) \rightarrow \Lambda_c^+ \bar{D}^0$	0.026	0.032	0.55	0.018	0.18	4.67
$p\psi(4415) \rightarrow \Lambda_c^+ \bar{D}^0$	0.0164	0.08	0.42	0.005	0.07	11.7
$p\psi(3770) \rightarrow \Lambda_c^+ \bar{D}^{*0}$	6.4	0.03	0.54	3.18	0.18	4.15
$p\psi(4040) \rightarrow \Lambda_c^+ \bar{D}^{*0}$	0.14	0.31	1.15	1.12	0.06	0.47
$p\psi(4160) \rightarrow \Lambda_c^+ \bar{D}^{*0}$	0.58	0.02	0.54	0.66	0.12	2.35
$p\psi(4415) \rightarrow \Lambda_c^+ \bar{D}^{*0}$	0.034	0.02	0.08	0.3	0.08	0.65
$p\psi(3770) \rightarrow \Sigma_c^{++} D^-$	0.017	0.07	0.93	0.021	0.05	0.35
$p\psi(4040) \rightarrow \Sigma_c^{++} D^-$	0.0067	0.071	0.51	0.004	0.19	38.6
$p\psi(4160) \rightarrow \Sigma_c^{++} D^-$	0.0012	0.01	0.35	0.0042	0.08	0.66
$p\psi(4415) \rightarrow \Sigma_c^{++} D^-$	0.0013	0.024	0.58	0.0022	0.168	4.29
$p\psi(3770) \rightarrow \Sigma_c^{++} D^{*-}$	0.012	0.04	0.01	5.4	0.058	0.48
$p\psi(4040) \rightarrow \Sigma_c^{++} D^{*-}$	0.34	0.03	0.64	0.53	0.19	2.33
$p\psi(4160) \rightarrow \Sigma_c^{++} D^{*-}$	0.13	0.017	5.92	0.85	0.058	0.5
$p\psi(4415) \rightarrow \Sigma_c^{++} D^{*-}$	0.007	0.0025	0.01	0.27	0.079	0.6
$p\psi(3770) \rightarrow \Sigma_c^+ \bar{D}^0$	0.005	0.1	0.38	0.014	0.04	0.47
$p\psi(4040) \rightarrow \Sigma_c^+ \bar{D}^0$	0.0009	0.01	0.29	0.0033	0.12	1.6
$p\psi(4160) \rightarrow \Sigma_c^+ \bar{D}^0$	0.00112	0.16	2.11	0.002	0.03	0.49
$p\psi(4415) \rightarrow \Sigma_c^+ \bar{D}^0$	0.0008	0.07	0.437	0.0006	0.162	9.3

Table 2: The same as Table 1, but for twenty other reactions.

reaction	a_1	b_1	c_1	a_2	b_2	c_2
$p\psi(3770) \rightarrow \Sigma_c^+ \bar{D}^{*0}$	1.4	0.01	0.52	2.6	0.1	1.21
$p\psi(4040) \rightarrow \Sigma_c^+ \bar{D}^{*0}$	0.041	0.0035	0.53	0.39	0.117	1.16
$p\psi(4160) \rightarrow \Sigma_c^+ \bar{D}^{*0}$	0.14	0.008	0.53	0.42	0.072	0.82
$p\psi(4415) \rightarrow \Sigma_c^+ \bar{D}^{*0}$	0.025	0.008	0.46	0.131	0.1	0.66
$p\psi(3770) \rightarrow \Sigma_c^{*++} D^-$	0.06	0.03	0.85	0.29	0.06	0.43
$p\psi(4040) \rightarrow \Sigma_c^{*++} D^-$	0.026	0.027	0.55	0.044	0.17	2.86
$p\psi(4160) \rightarrow \Sigma_c^{*++} D^-$	0.0446	0.054	0.45	0.003	0.234	82.8
$p\psi(4415) \rightarrow \Sigma_c^{*++} D^-$	0.0037	0.24	0.21	0.013	0.07	0.63
$p\psi(3770) \rightarrow \Sigma_c^{*++} D^{*-}$	0.4	0.09	3.24	1	0.06	0.4
$p\psi(4040) \rightarrow \Sigma_c^{*++} D^{*-}$	0.0058	0.0038	0.38	0.0967	0.158	1.34
$p\psi(4160) \rightarrow \Sigma_c^{*++} D^{*-}$	0.05	0.02	0.61	0.17	0.08	0.52
$p\psi(4415) \rightarrow \Sigma_c^{*++} D^{*-}$	0.034	0.059	2.62	0.038	0.29	0.32
$p\psi(3770) \rightarrow \Sigma_c^{*+} \bar{D}^0$	0.005	0.013	9.57	0.178	0.059	0.49
$p\psi(4040) \rightarrow \Sigma_c^{*+} \bar{D}^0$	0.012	0.212	8.38	0.021	0.066	0.45
$p\psi(4160) \rightarrow \Sigma_c^{*+} \bar{D}^0$	0.0073	0.0161	1.5	0.019	0.061	0.4
$p\psi(4415) \rightarrow \Sigma_c^{*+} \bar{D}^0$	0.0002	0.001	0.5	0.0082	0.08	0.57
$p\psi(3770) \rightarrow \Sigma_c^{*+} \bar{D}^{*0}$	0.148	0.186	4.97	0.583	0.0477	0.514
$p\psi(4040) \rightarrow \Sigma_c^{*+} \bar{D}^{*0}$	0.0057	0.008	0.55	0.065	0.164	2.08
$p\psi(4160) \rightarrow \Sigma_c^{*+} \bar{D}^{*0}$	0.037	0.013	0.33	0.1	0.09	1.25
$p\psi(4415) \rightarrow \Sigma_c^{*+} \bar{D}^{*0}$	0.003	0.014	0.18	0.026	0.1	0.71